Plant Communications
Research Article

CellPress
Partner Journal

Abscisic Acid Connects Phytohormone Signaling with RNA Metabolic Pathways and Promotes an Antiviral Response that Is Evaded by a Self-Controlled RNA Virus

Fabio Pasin[1,2,*], Hongying Shan[1,6], Beatriz García[1], Maren Müller[3], David San León[1], Márta Ludman[4], David H. Fresno[3], Károly Fátyol[4], Sergi Munné-Bosch[3], Guillermo Rodrigo[5] and Juan Antonio García[1]

[1]Centro Nacional de Biotecnología (CNB-CSIC), 28049 Madrid, Spain

[2]Agricultural Biotechnology Research Center, Academia Sinica, 11529 Taipei, Taiwan

[3]Departamento de Biología Evolutiva, Ecología y Ciencias Ambientales, Facultad de Biología, Universidad de Barcelona, 08028 Barcelona, Spain

[4]Agricultural Biotechnology Institute, National Agricultural Research and Innovation Centre, 2100 Gödöllő, Hungary

[5]Institute for Integrative Systems Biology (I2SysBio), CSIC-University of Valencia, 46980 Paterna, Spain

[6]Present address: College of Horticulture and Gardening, Tianjin Agricultural University, 300384 Tianjin, China

***Correspondence: Fabio Pasin (fpasin@cnb.csic.es)**

https://doi.org/10.1016/j.xplc.2020.100099

ABSTRACT

A complex network of cellular receptors, RNA targeting pathways, and small-molecule signaling provides robust plant immunity and tolerance to viruses. To maximize their fitness, viruses must evolve control mechanisms to balance host immune evasion and plant-damaging effects. The genus *Potyvirus* comprises plant viruses characterized by RNA genomes that encode large polyproteins led by the P1 protease. A P1 autoinhibitory domain controls polyprotein processing, the release of a downstream functional RNA-silencing suppressor, and viral replication. Here, we show that P1Pro, a plum pox virus clone that lacks the P1 autoinhibitory domain, triggers complex reprogramming of the host transcriptome and high levels of abscisic acid (ABA) accumulation. A meta-analysis highlighted ABA connections with host pathways known to control RNA stability, turnover, maturation, and translation. Transcriptomic changes triggered by P1Pro infection or ABA showed similarities in host RNA abundance and diversity. Genetic and hormone treatment assays showed that ABA promotes plant resistance to potyviral infection. Finally, quantitative mathematical modeling of viral replication in the presence of defense pathways supported self-control of polyprotein processing kinetics as a viral mechanism that attenuates the magnitude of the host antiviral response. Overall, our findings indicate that ABA is an active player in plant antiviral immunity, which is nonetheless evaded by a self-controlled RNA virus.

Keywords: abscisic acid, antiviral immune evasion, mathematical modeling, viral polyprotein processing, *Potyvirus*, RNA metabolism

Pasin F., Shan H., García B., Müller M., San León D., Ludman M., Fresno D.H., Fátyol K., Munné-Bosch S., Rodrigo G., and García J.A. (2020). Abscisic Acid Connects Phytohormone Signaling with RNA Metabolic Pathways and Promotes an Antiviral Response that Is Evaded by a Self-Controlled RNA Virus. Plant Comm. **1**, 100099.

INTRODUCTION

Recent surveys underscore the great abundance and diversity of plant viruses that pose major challenges to host defense pathways and, thus, to plant health and food security (Pasin et al., 2019). Multiple layers of defense and complex networks of receptors, small molecules, and transcriptional regulators provide robust plant immunity and tolerance to pathogens (Nakahara and

Published by the Plant Communications Shanghai Editorial Office in association with Cell Press, an imprint of Elsevier Inc., on behalf of CSPB and IPPE, CAS.

Masuta, 2014; Tsuda and Somssich, 2015; Jeon et al., 2017; Nobori et al., 2018; Paudel and Sanfaçon, 2018; Murphy et al., 2020). Salicylic acid (SA) is a defense phytohormone that mediates resistance to biotrophic pathogens and interacts antagonistically or synergistically with other host small molecules (Berens et al., 2017). SA biosynthesis and signaling are activated during the hypersensitive response (HR) to viruses and are integrated in emerging models of plant immunity to viruses (Nakahara and Masuta, 2014; Alazem and Lin, 2015; Murphy et al., 2020). Viruses in turn have evolved strategies to repress or evade antiviral HR and SA-dependent resistance (Nakahara and Masuta, 2014). In accordance with these models, members of the families *Caulimoviridae*, *Bromoviridae*, *Potyviridae*, *Tombusviridae*, and *Virgaviridae* are known to interfere with SA pathways by mechanisms already reviewed (Nakahara and Masuta, 2014; Alazem and Lin, 2015; Yang and Li, 2018; Murphy et al., 2020; Shen et al., 2020).

Evidence indicates that RNA silencing and small-molecule signaling cooperate to promote plant resistance to viruses (Alazem and Lin, 2015, 2020; Yang and Li, 2018; Murphy et al., 2020; Yang et al., 2020). Whereas early studies focused on the interplay of RNA silencing and SA, an increasing body of data supports the contribution of other phytohormones, such as abscisic acid (ABA), to antiviral responses (Pacheco et al., 2012; Chen et al., 2013, 2017; Westwood et al., 2013; Seo et al., 2014; Alazem et al., 2017; Zhang et al., 2019; Alazem and Lin, 2020). Defects in RNA-silencing components that contribute to antiviral immunity were shown to enhance sensitivity to ABA, as reported for the *Arabidopsis thaliana* mutant lines of HYPONASTIC LEAVES 1 (HYL1), HUA ENHANCER 1 (HEN1), ARGONAUTE1 (AGO1), and DICER-LIKE (DCL) proteins (Zhang et al., 2008), reviewed in Alazem and Lin (2020). In addition to RNA silencing, several pathways control RNA maturation and turnover in plant cells, and their impact on virus infection dynamics has just begun to be appreciated (Mäkinen et al., 2017; Chantarachot and Bailey-Serres, 2018; Boudreault et al., 2019; Xu et al., 2020). For instance, RNA decay was recently reported to act in concert with RNA silencing to promote antiviral immunity in plants (Li and Wang, 2018, 2019). Studies have highlighted connections between osmotic stress responses, ABA signaling, and RNA decay (Kawa and Testerink, 2017; Soma et al., 2017; Wawer et al., 2018); however, the biological significance of the interplay between ABA and RNA metabolic pathways (beyond RNA silencing) in plant antiviral immunity remains largely unexplored.

Viruses are obligate parasites that adopt distinct translational strategies to maximize the coding capacity of their small genomes. Polyprotein synthesis from long open reading frames is one of the most common strategies used by RNA viruses. Large polypeptide precursors are synthesized, and the release of functional viral gene products is mediated by polyprotein processing. Many viral agents of human and veterinary infectious diseases, and almost half of known plant viruses, rely on proteolytic cleavage events as key co- and post-translational modifications throughout their infection cycle (Yost and Marcotrigiano, 2013; Rodamilans et al., 2018; Mann and Sanfaçon, 2019). Virus-encoded proteases are multifunctional hubs that coordinate virus replication and host–virus interactions to promote infectivity and virulence (Martínez et al., 2016; Lei and Hilgenfeld, 2017; Rodamilans et al., 2018). The spatial-temporal regulation of protease activity and the processing of viral polyproteins can further determine viral persistence and disease lethality (Lackner et al., 2004; Yost and Marcotrigiano, 2013; Isken et al., 2019).

Polyproteins are synthesized by members of the picornavirus supergroup that includes *Potyviridae*, the largest family of plant RNA viruses (Revers and García, 2015). Most potyvirids have narrow host ranges, and their leader P1 proteases show considerable sequence variability linked to host adaptation (Cui and Wang, 2019). P1 self-cleaves from viral polyproteins and the mature P1 lacks *trans*-cleavage activity (Cui and Wang, 2019). P1 self-cleavage defects impair the RNA-silencing suppressor activity of the downstream protein element HCPro and preclude virus infectivity (Verchot and Carrington, 1995; Pasin et al., 2014; Shan et al., 2015). Deletion mutagenesis and *in vitro* assays enabled mapping of the core C-terminal protease domain of P1 and showed that its N terminus negatively regulates the self-cleavage activity (Pasin et al., 2014; Shan et al., 2018). The N terminus is therefore an autoinhibitory domain that controls P1 self-cleavage and HCPro release. *In vitro* assays indicated that P1 autoinhibition is alleviated by an unknown host factor. Consistent with these results, removal of the P1 N terminus boosted *in vivo* P1 self-cleavage and local viral amplification in a non-permissive host (Shan et al., 2018). In viral infections of permissive hosts, removal of the P1 autoinhibitory domain accelerated early replication and enhanced symptom severity, which were accompanied by a later drop in viral load (Pasin et al., 2014).

Here, we used a plum pox virus (PPV) (genus *Potyvirus*) isolate adapted to infect herbaceous hosts to investigate the contribution of viral leader proteases and polyprotein processing to virus–host interactions and pathogen fitness. P1Pro is a PPV clone that lacks the autoinhibitory domain of the P1 leader protease and has an uncontrolled release of the viral-silencing suppressor HCPro. HCPro release and proteolytic activity of the truncated P1 version encoded by P1Pro was confirmed *in vitro* and *in planta*, including in non-host plant species (Shan et al., 2018). P1Pro infection was found to elicit HR and to induce the accumulation of pathogenesis-related (PR) proteins, including PR-2 and PR-3. This induction was considerably reduced but not eliminated in a transgenic *N. benthamiana nahG* line that expresses an SA hydroxylase gene (Pasin et al., 2014). We reasoned that SA and uncharacterized defense components could participate in P1Pro-activated responses. In this study, host molecular changes triggered by P1Pro were further characterized using a transcriptomic approach. Our results support the role of SA as a major defense phytohormone involved in antiviral responses. Analysis of SA-defective plants uncovered ABA as an additional antiviral component that contributes to potyviral resistance. To provide an understanding of the ABA effects on antiviral immunity, public datasets of *A. thaliana* transcriptomes and phosphoproteomes were analyzed. ABA treatments affected the phosphorylation status of RNA metabolic components, including those involved in RNA cap binding, maturation, decay, and translation initiation. Genetic and hormone treatment assays showed that ABA promotes plant resistance to PPV infection. Together, our results suggest that an ABA-dependent, genome-wide perturbation of host RNA metabolism can promote an antiviral response that is evaded by a self-controlled RNA virus. Finally, we developed a mathematical model supporting the

mechanistic relationships among the controlled processing of viral polyproteins, the strength of the silencing suppression, the activation of host hormonal responses, and overall virus fitness.

RESULTS

P1Pro Infection Elicits SA Accumulation

The P1Pro clone is a PPV deletion mutant lacking the N-terminal autoinhibitory domain that controls the self-cleavage of the P1 leader protease (Figure 1A). Wild-type and SA-defective (*nahG*) lines of *N. benthamiana* were used as hosts to study defense responses elicited by P1Pro infection; mock- or PPV-treated plants were used as controls. Analysis of upper uninoculated leaves showed significantly increased free SA in P1Pro-infected wild-type host samples compared with mock- or PPV-treated plants (wild-type or *nahG*) or *nahG* plants inoculated with P1Pro ($p < 0.01$; Figure 1B). The result confirmed SA as a major contributor to P1Pro-activated responses.

P1Pro Infection Reprograms the Host Transcriptome

The transcriptomes of wild-type *N. benthamiana* plants inoculated with PPV or P1Pro clones (PPV+ and P1Pro+ samples, respectively) were analyzed by Illumina RNA sequencing (RNA-seq). *N. benthamiana nahG* plants inoculated with P1Pro (P1Pro−) were further analyzed to identify genes whose expression is altered by P1Pro infection but does not depend on SA signaling (Figure 1B). For each condition, three biological replicates were analyzed. Sequencing reads were mapped to the PPV genome and to the *nahG* transgene as preliminary quality control (Supplemental Figure 1A; see Supplemental Information). Coverage of the full-length P1 sequence was obtained for PPV samples, whereas P1Pro samples showed a coverage gap in the 5′ end corresponding to the P1 truncation. Samples from the transgenic *N. benthamiana* line showed high *nahG* coverage and confirmed the host genotypes used. Reads were further mapped to an *N. benthamiana* transcriptome version (Nakasugi et al., 2014). To assess sample consistency and host-response similarities, count values were subjected to an unsupervised multivariate analysis. Representation of principal components showed a clear separation between the three conditions analyzed (i.e., PPV+, P1Pro+, and P1Pro−) and correct grouping of their biological replicates (Figure 1C). Hierarchical clustering and bootstrap analysis corroborated the results with approximately unbiased confidence of $\geq$ 99% (Supplemental Figure 1B). To identify statistically significant differentially expressed genes, transcript count values were used in two-way comparisons to compute false discovery rate (FDR) values. The PPV+, P1Pro+, and P1Pro− datasets were thus analyzed to yield three different two-way comparisons (see Supplemental Data 1A). Transcripts were filtered based on FDR < 0.05 and, to further explore sample similarities, count values of transcripts that were differentially expressed in at least one comparison were used to calculate pairwise correlation coefficients between samples. Consistent with the principal component analysis, samples from the same condition showed a high correlation ($r > 0.96$), whereas correlations were lower between conditions, ranging from 0.76 to 0.94 (Supplemental Figure 1C).

The magnitude of expression profile changes showed that, in wild-type hosts and using the PPV clone as a reference, P1Pro infections were dominated by gene upregulation (538 of 757 genes in the P1Pro+/PPV+ comparison; Figure 1D and Supplemental Data 1A). The median fold change of the P1Pro+/PPV+ comparison was greater than those of the P1Pro−/PPV+ and P1Pro−/P1Pro+ comparisons. Hierarchical clustering using read counts of the differentially expressed transcripts showed major sample clusters that corresponded to the three conditions analyzed (Figure 1E). Heatmap visualization and the clustering of individual transcripts further highlighted specific groups of genes that were up- and, in a few cases, downregulated by P1Pro versus PPV infections in the wild-type host (P1Pro+ versus PPV+; Figure 1E). The expression profiles of these gene groups were largely divergent in P1Pro infections of the *nahG* plants (P1Pro+ versus P1Pro−). These findings indicate that, in P1Pro+ samples, the abundance of a large set of transcripts significantly deviates from that of wild-type virus infections or P1Pro-infected hosts with defective SA signaling.

P1Pro Infection Alters the Expression of SA-Related Defense Genes and Transcription Factors Associated with Diverse Signaling Pathways

To confirm the role of SA and identify additional defense components that may be associated with P1Pro infection, we analyzed transcripts that showed differential expression in the P1Pro+/PPV+ comparison. Functional annotations were made using the proteome of the model plant *Arabidopsis thaliana* (Supplemental Data 1A) and its associated gene ontology (GO) terms, or a custom sequence list that covered reported PR families (Supplemental Data 1B). Specific GO categories were overrepresented and showed partial overlaps in windows of genes that were significantly up- or downregulated by P1Pro (Figure 1F). Upregulated genes were enriched in stress response terms, including "response to biotic stimulus" and "defense response"; conversely, downregulated genes were associated with the terms "chloroplast" and "photosynthesis" (Figure 1F). P1Pro upregulated several genes associated with SA signaling, including *NPR3* homologs and a wide array of *PR* genes from different families (Supplemental Figure 2). Pipecolic acid is a metabolite that can act synergistically with SA to promote plant immunity (Hartmann and Zeier, 2019; Wang et al., 2019); homologs of its core signaling components *ALD1*, *WRKY33*, and *SARD1* were also upregulated in P1Pro samples. RNA-silencing components, including *AGO1* and *AGO2*, were downregulated in P1Pro samples (Supplemental Figure 2).

Transcription factors (TFs) were specifically examined because they transmit information signals to reprogram host transcriptomes and modulate immune responses (Tsuda and Somssich, 2015). In addition to *WRKY33* and *SARD1*, members of several TF families with known roles in plant immunity, including the AP2/ERF, bHLH, MYB, NAC, and WRKY families, were differentially expressed in P1Pro versus PPV infections (Supplemental Figure 2). Like the 757 differentially expressed transcripts (ALL) identified in the P1Pro+/PPV+ comparison, TFs were distributed across different expression windows, and the majority were upregulated (Figure 1G and Supplemental Figure 2). We hypothesized that selective enrichment of GO terms associated with TFs would provide insight into signals activated by P1Pro. Combined functional analyses of the complete list of ALL transcripts and the TF subset supported the role of SA in P1Pro

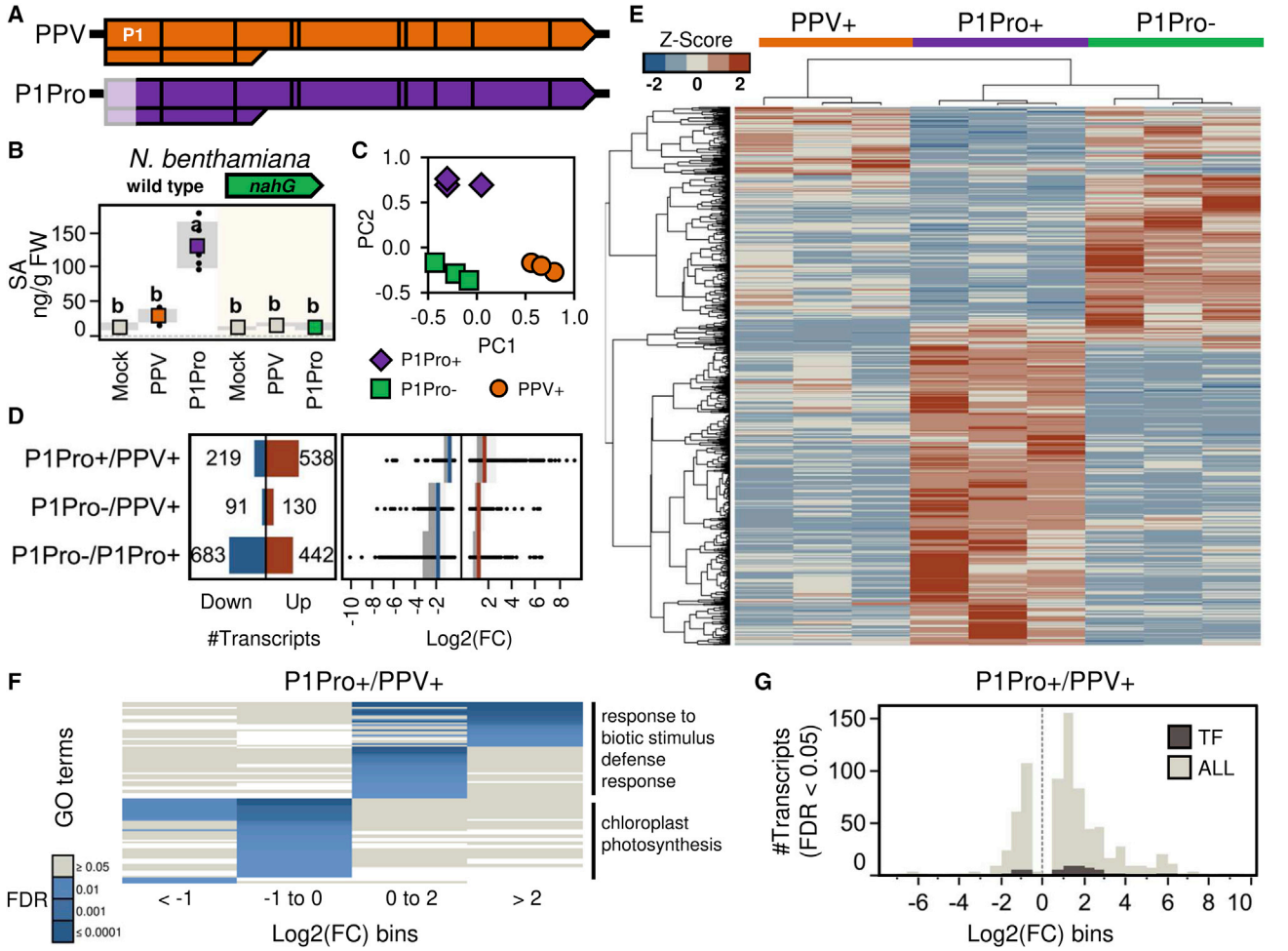

Figure 1. Transcriptomic Changes in Host Plants Infected with PPV and Its Deletion Mutant P1Pro.

(A) Genome representation of wild-type PPV or P1Pro, a PPV clone that lacks the N-terminal autoinhibitory domain of the P1 protease. The green fluorescent protein (*GFP*) gene, located between the NIb and CP cistrons of both viral clones, is omitted for clarity.

(B) Quantification of SA in plants inoculated with PPV or P1Pro clones; wild-type *Nicotiana benthamiana* and a transgenic line expressing a salicylate hydroxylase gene (*nahG*) were used as host plants. The plot shows mean ± SD (boxes and shadows, respectively; $n = 5$); letters indicate $p < 0.01$, one-way ANOVA and Tukey's honestly significant difference (HSD) test. Conditions in color (orange, purple, and green) were analyzed by RNA-seq with three biological replicates per condition.

(C) Principal component analysis of the samples analyzed by transcriptomics.

(D) Total number (left) and fold change (right) of differentially expressed transcripts (FDR < 0.05); fold change medians are indicated by colored lines.

(E) Normalized read counts of differentially expressed transcripts and their clustering analysis; for each condition, the values of different biological replicates are shown. PPV+ and P1Pro+ denote wild-type *N. benthamiana* plants agroinoculated with PPV and P1Pro clones, respectively; P1Pro, *nahG*-expressing *N. benthamiana* plants agroinoculated with P1Pro.

(F) Enrichment of functional categories in genes differentially regulated by P1Pro with respect to PPV in the wild-type host (P1Pro+/PPV+ comparison); representative gene ontology (GO) terms across fold change windows are indicated (right).

(G) Fold change distribution (bins of 0.5) of differentially expressed transcripts (ALL) or only those that encoded transcription factors (TFs) identified in the P1Pro+/PPV+ comparison.

responses (GO:0009751, GO:0009627) and highlighted putative contributions of the phytohormones jasmonic acid, ethylene, auxin, and gibberellin, as well as components involved in abiotic stress signaling (GO:0009628, GO:0009414, GO:0047484; Supplemental Figure 3).

Salicylate-Dependent and -Independent Immune Responses Are Elicited by P1Pro Infection

Functional analysis indicates that SA and unknown phytohormone(s) might contribute to P1Pro responses. SA depletion in *nahG*-expressing plants is predicted to alter transcriptional regulation of genes linked to SA signaling, whereas the expression of SA-independent genes should be unaffected. The transcriptomes of PPV+ and P1Pro+ samples were compared with those of P1Pro-inoculated *N. benthamiana nahG* plants (P1Pro−). Expression profiles of wild-type or *nahG* plants infected with P1Pro (P1Pro+ and P1Pro−, respectively) were significantly divergent (Figure 1C–1E and Supplemental Figure 1B). Relationships of lists of differentially expressed genes were analyzed (Figure 2A and Supplemental Data 1A). The intersection of the P1Pro+/PPV+ and P1Pro−/P1Pro+ sets

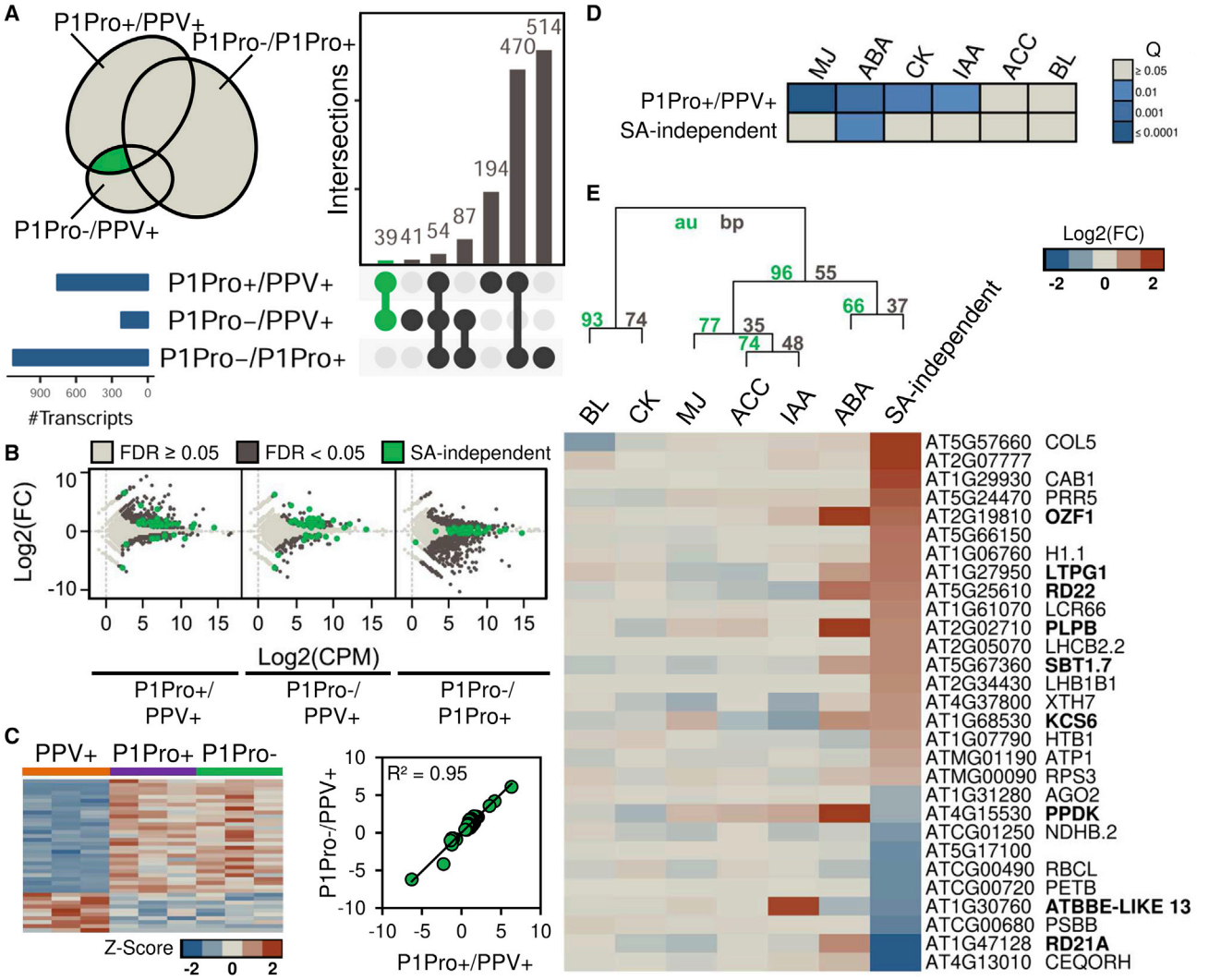

Figure 2. SA-Dependent and -Independent Transcriptomic Changes in P1Pro-Infected Plants.

(A) Comparisons of lists of differentially expressed genes (FDR < 0.05). The Venn diagram shows spatial relationships between gene lists; the numbers of overlapping genes are indicated (right). The green intersection highlights a subset of genes that are altered in P1Pro-infected wild-type plants but not in *nahG*-transgenic plants (where SA signaling is downregulated; i.e., SA-independent genes).

(B) Fold change and coverage plots of transcriptomic data; SA-independent genes are colored green.

(C) Left, normalized read counts (heatmap; $n = 3$) and, right, correlation plot of fold changes for the SA-independent genes in wild-type or *nahG*-transgenic plants infected with P1Pro (P1Pro+ and P1Pro−, respectively), using the PPV+ condition as a reference.

(D) The SA-independent set significantly overlaps ABA marker genes. *A. thaliana* homologs of the differentially expressed genes in *N. benthamiana* were identified by BLASTX searches. Lists obtained were confronted against hormone marker genes from public *A. thaliana* microarrays (MJ, methyl jasmonate; ABA; CK, zeatin; IAA, indole-3-acetic acid; ACC, aminocyclopropane-1-carboxylic acid; BL, brassinolide). The color scale shows overlap significance based on the hypergeometric test.

(E) Hierarchical clustering and fold changes of the SA-independent gene set identified by our RNA-seq and microarrays from hormone-treated *A. thaliana* plants. Cluster probabilities are indicated (au, approximately unbiased; bp, bootstrap probability). Symbols of genes whose expression is significantly altered ($p < 0.01$) in ABA-treated *A. thaliana* seedlings are in boldface.

included 524 genes (bars labeled with 470 plus 54 in Figure 2A); of these, 48 were identified as *PR* genes. Compared with the union set, this functional enrichment was significantly higher than expected by chance ($Q = 3.54 \times 10^{-7}$), indicating that the regulation of *PR* gene expression depends both on the virus clones and functional SA signaling in the host.

The intersection of P1Pro+/PPV+ and P1Pro−/PPV+ sets revealed 39 elements outside the P1Pro−/P1Pro+ list, implying that their regulation depends on the virus clones used but does not require SA signaling (i.e., SA-independent genes; green in Figure 2A; Supplemental Table 1 and Supplemental Data 1A). Visual inspection of the fold change plots of P1Pro+/PPV+ and P1Pro−/PPV+ comparisons confirmed that elements of the SA-independent set were distributed in the space associated with significantly up- or downregulated transcripts (FDR < 0.05); conversely, they lay close to the x axis (i.e., fold change ~ 0 and FDR ≥ 0.05) in the P1Pro−/P1Pro+ plot (Figure 2B).

SA-independent transcripts showed similar read counts in the P1Pro+ and P1Pro− conditions and diverged from PPV+ samples, and their fold changes using PPV+ values as reference were strongly correlated (R^2 = 0.95; Figure 2C).

Compared with *N. benthamiana*, rich public datasets are available for the model plant *A. thaliana.* The SA-independent transcripts we identified were mapped to 29 *A. thaliana* homologs, and these were compared with hormone marker genes from a transcriptomic study of *A. thaliana* (Nemhauser et al., 2006). This meta-analysis showed that the SA-independent genes showed significantly greater overlap with ABA markers than expected by chance (nine genes, Q = 0.010; Figure 2D). Fold change values from the *A. thaliana* transcriptomic study and our RNA-seq analysis, as well as hierarchical clustering, supported grouping of the ABA and SA-independent sets (Figure 2E). Among the *A. thaliana* ABA-responsive genes (boldface, Figure 2E) and compared with our data, the expression values of the two markers were discordant, whereas the expression change of the remainder coincided (*OZF1*, *LTPG1*, *RD22*, *PLPB*, *SBT1.7*, *KCS6*, and *ATBBE-LIKE 13*).

Removal of the P1 Autoinhibitory Domain Triggers ABA Accumulation in Viral Infection but Is Itself Insufficient to Activate Local HR

In *N. benthamiana* compared with mock-treated or PPV-infected plants, P1Pro infection triggered HR that was accompanied by enhanced accumulation of the *OZF1* homolog *NbOZF1* and ABA ($p < 0.01$; Figure 3A). In *A. thaliana*, expression of the *OZF1* zinc finger protein gene is activated by ABA in vegetative tissues (Lee et al., 2012), and its protein was recently shown to be a preferential target of multiple secreted effectors from *Pseudomonas syringae* (Cao et al., 2019). We asked whether the truncated P1 version encoded by the P1Pro clone and lacking the N-terminal autoinhibitory domain was sufficient to activate effector-triggered immunity (ETI), thereby causing HR. Transient expression of the P1 N-terminal deletion construct, either alone or as a part of a polyprotein including HCPro, was not sufficient to activate HR, as was apparent in *N. benthamiana* leaves infiltrated with a bacterial effector construct (avr; Figure 3B).

AGO2 Depletion Is Sufficient to Enhance ABA Levels during Potato Virus X Infection but Not upon Infection with the Self-Controlled, Wild-Type PPV

ABA has been proposed to promote antiviral defenses through the transcriptional regulation of RNA-silencing genes, including *AGO2* (Alazem and Lin, 2020). *AGO2* was identified in the SA-independent set of differentially expressed transcripts in our RNA-seq data. Compared with PPV samples, P1Pro infection showed high ABA levels (Figure 3A) and reduced AGO2 transcript and protein levels (Figure 2E and Supplemental Figure 2; Supplemental Tables 1 and 2). Microarray analysis nonetheless indicated that ABA was insufficient to enhance *AGO2* expression in *A. thaliana* seedlings at 3 h post-treatment (Figure 2E). Time series RNA-seq data from *A. thaliana* seedlings treated with ABA showed that *OZF1* and *PP2CA*, a known component of ABA signaling in vegetative tissues, were upregulated by 10 μM ABA within 1 h post-treatment (FDR < 0.01). Conversely, *AGO2* expression showed no significant changes during the 60 h assay (Figure 3C). Microarray analysis of hormone-treated *A. thaliana* plants further showed that transcript abundance of the main RNA-silencing components, i.e., *AGO*, *RDR*, and *DCL*, was largely unaltered by ABA or other phytohormones (Figure 3D; note that the effects of SA were not analyzed).

To further test whether *AGO2* regulation and ABA signaling were related, we measured ABA amount in an *ago2* knockout line of *N. benthamiana*. The *ago2* plants inoculated with P1Pro showed high ABA and SA levels (Figure 3E), indicating that induction of ABA and SA accumulation does not require AGO2. Based on our working model, host defenses are activated by uncontrolled silencing suppression activity of the P1Pro clone. We asked whether, in a complementary approach, *ago2* depletion might be sufficient to trigger ABA accumulation during wild-type virus infections. Wild-type and *ago2* plants were therefore inoculated with PPV. Potato virus X (PVX) was also included because a recombinant PVX clone expressing HCPro of PPV was previously shown to trigger ABA accumulation in *N. benthamiana* plants; this effect was dependent on the silencing suppressor activity of HCPro (Pacheco et al., 2012). Mock-treated wild-type and *ago2* plants showed similar phytohormone amounts, indicating that AGO2 absence is itself insufficient to activate ABA or SA. Irrespective of the host genotype used, no significant changes in ABA levels were detected in PPV infections. The ABA and SA amounts in the PVX-infected *ago2* host were significantly higher than in the other conditions (Figure 3F). These results showed that (1) *AGO2* and major RNA-silencing genes are not primary transcriptional targets of ABA signaling; (2) the perturbation of RNA silencing triggers ABA accumulation during P1Pro or PVX infections; and (3) by contrast, viral control of silencing suppressor activity avoids the activation of ABA signaling during PPV infection in both wild-type and RNA-silencing-defective hosts.

ABA Regulates the Protein Phosphorylation Dynamics of RNA Metabolic Components

ABA coordinates plant responses to osmotic stress, and its perception is mediated by PYR/PYL receptors that selectively bind and inhibit PP2C protein phosphatases in the presence of ABA. This in turn allows the activation of SnRK2 kinases and the phosphorylation of downstream TFs (Cutler et al., 2010). We asked whether ABA signaling could affect host antiviral RNA-silencing components at a post-translational level. Public data from *A. thaliana* phosphoproteomes were analyzed (Umezawa et al., 2013; Wang et al., 2013, 2020; Mergner et al., 2020). We considered a subset of proteins redundantly identified in at least two independent phosphoproteomic datasets from plants treated with ABA or subjected to osmotic stress (Supplemental Data 1C). This responsive subset, which accounted for 9.21% of known phosphoproteins (Figure 4A), was also characterized by a high phosphorylation level of predicted phosphosites in untreated conditions (Figure 4B), and included none of the major RNA-silencing components (Supplemental Figure 4). We concluded that the transcriptional and post-translational regulation of antiviral RNA silencing is largely independent of ABA signaling (Figure 3D and Supplemental Figure 4).

The functional analysis of the identified subset revealed enrichment in GO terms related to RNA metabolism, including

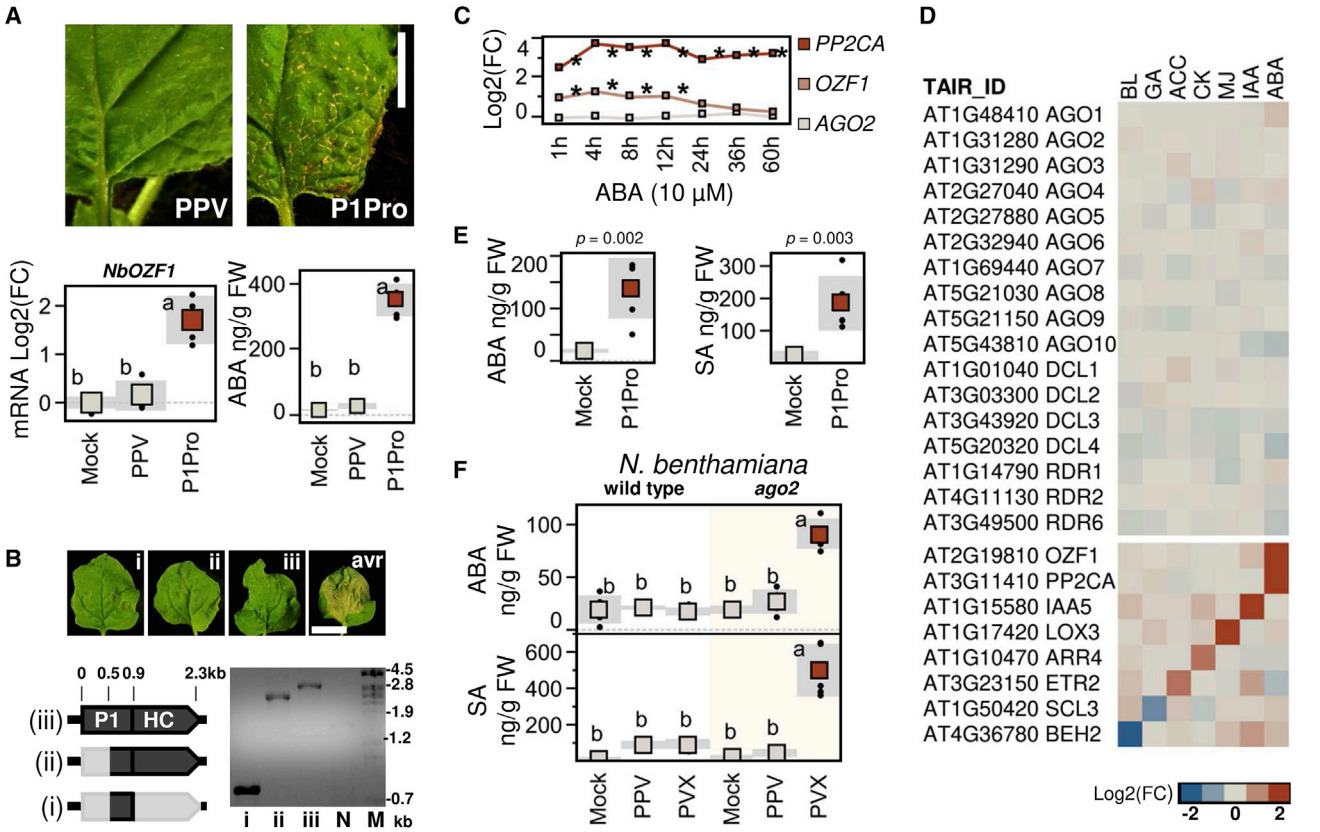

Figure 3. The Self-Controlled, Wild-Type PPV Evades the Activation of ABA Signaling during Plant Infection.

(A) Symptoms of upper uninoculated leaves of wild-type plants inoculated with PPV or P1Pro. Scale bar corresponds to 1 cm. Plots show the qRT–PCR quantification of *NbOZF1* (mean ± SD, $n = 4$) and ABA amounts (mean ± SD, $n = 6$); letters indicate $p < 0.01$, one-way ANOVA and Tukey's HSD test.

(B) Transient expression of (i) N-terminally truncated P1, (ii) N-terminally truncated P1 and HCPro, and (iii) full-length P1 and HCPro constructs; avr indicates the HopAB2 construct that was used as a positive control of HR. Images of leaves were taken at 6 days post-agroinoculation (dpa). Scale bar corresponds to 2 cm. The gel shows the RT–PCR analysis of infiltrated leaves using primers that anneal to the 5′ and 3′ UTR of the constructs. N, non-infiltrated sample; M, DNA size marker.

(C) Time course analysis of *OZF1* and *AGO2* fold changes in the public RNA-seq datasets of ABA-*treated A. thaliana* seedlings; *PP2CA* serves as an ABA-responsive control; *FDR < 0.01.

(D) Transcriptional regulation of the main RNA-silencing genes by phytohormones. Transcript fold changes from the public microarray data of *A. thaliana* seedlings treated for 3 h with BL, gibberellic acid (GA), ACC, CK, MJ, IAA, or ABA are shown. *OZF1*, *PP2CA*, *IAA5*, *LOX3*, *ARR4*, *ETR2*, *SCL3*, and *BEH2* are included as hormone-responsive control genes.

(E) *N. benthamiana ago2* plants were inoculated with P1Pro or mock treated. ABA and SA amounts at 7 dpi are plotted (mean ± SD, $n = 5$); p values are shown (Student's t-test).

(F) PPV and potato virus X (PVX) were delivered to wild-type or *ago2*-mutant plants; ABA and SA amounts are plotted (mean ± SD, $n = 5$); letters indicate $p < 0.01$, one-way ANOVA and Tukey's HSD test. Viruses were delivered to *N. benthamiana* plants by mechanical inoculation and transient expression constructs by *Agrobacterium* infiltration.

RNA processing, splicing, and translation (Figure 4C). Multiple proteins involved in plant RNA metabolism are known (Kawa and Testerink, 2017; Chantarachot and Bailey-Serres, 2018). The phosphorylation status of several components of RNA cap-binding complexes that coordinate host mRNA stability and translation initiation was altered by ABA and osmotic stress (Figure 4D). These treatments also altered the phosphorylation of RNA decay and mRNA turnover regulators.

ABA and P1Pro Infection Alter Plant RNA Diversity

Close inspection of the identified phosphoproteome subset showed proteins involved in pre-mRNA splicing, such as serine/arginine-rich splicing factors, components of the cap-binding complex and those necessary for spliceosomal complex assembly (Supplemental Figure 5A). Consistent with these findings and a regulatory role of ABA in plant RNA maturation and diversity (Laloum et al., 2018), the use of a robust bioinformatic workflow (see Supplemental Information) and time series RNA-seq datasets from *A. thaliana* enabled the quantification of alternative splice (AS) events significantly altered by ABA (Supplemental Data 1D). Classification of the AS types identified skipping exon (SE), retained intron (RI), mutually exclusive exon (MX), and alternative 5′ or 3′ splice site (A5, A3) events, and showed that RI was the predominant type (Figure 4E). Differentially expressed genes and those presenting AS events showed low overlap and different dynamics; a large increase in differentially expressed genes was observed at 4 h, whereas the number of

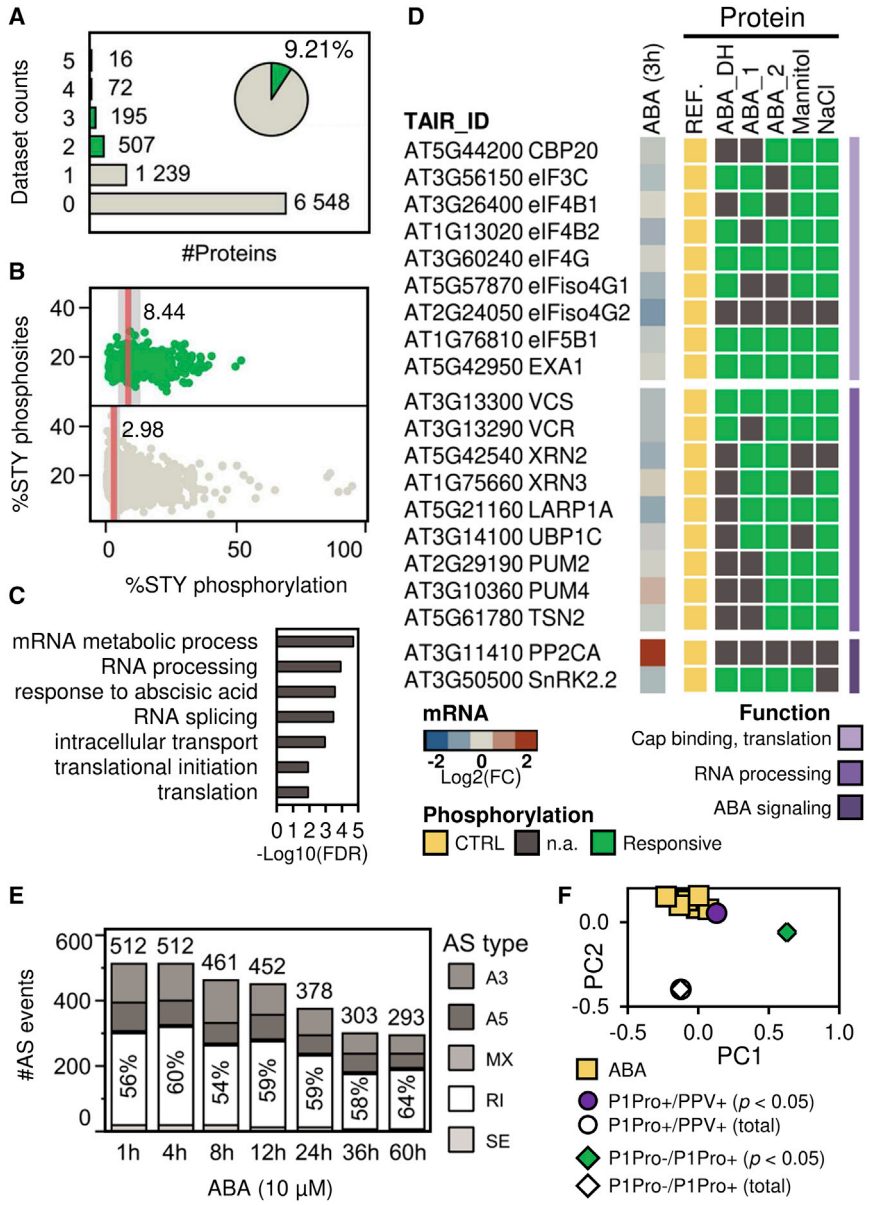

Figure 4. ABA Modulates the Phosphorylation Dynamics of RNA Cap-Binding and Processing Complex Components and Host Transcriptomic Diversity.

Public phosphoproteomic datasets, including *A. thaliana* proteins whose phosphorylation status is significantly altered by ABA and dehydration (ABA_DH), ABA (ABA_1, ABA_2), mannitol, or NaCl were analyzed; a comprehensive phosphoproteome was used as a control of known phosphoproteins (REF.; see Supplemental Data 1C).

(A) Overlap of phosphoproteomic datasets. Proteins identified in at least two treatment datasets were considered the responsive subset (green).

(B) Predicted serine, threonine, and tyrosine (STY) phosphosites and their phosphorylation status in proteins identified in the responsive subset (green, top) or a reference phosphoproteome (bottom). Median values are indicated.

(C) Representative GO terms enriched in the responsive subset proteins.

(D) Transcriptional and post-translational regulation of the components of cap-binding and RNA processing complexes. For each *A. thaliana* gene accession, the heatmap shows microarray expression values from ABA-treated seedlings at 3 h (left) and their protein phosphorylation status and functional annotations (right). Proteins identified in the treatment (responsive) and control phosphoproteome datasets (CTRL) are shown; n.a., no change or phosphopeptide identified. PP2CA and SnRK2.2 are included as ABA-responsive transcriptional or post-translational markers, respectively.

(E) Time course analysis of alternative splicing (AS) events significantly altered (adjusted $p < 0.05$) in ABA-treated *A. thaliana* seedlings. Event numbers and the ratios of AS types are shown; SE, skipping exon; RI, retained intron; MX, mutually exclusive exon; A5, alternative 5′ splice site; A3, alternative 3′ splice site.

(F) Principal component analysis of SE, MX, A5, A3, and the RI ratios of events shown in **(E)** (ABA; each point of the time-course analysis is plotted) or altered in *N. benthamiana* P1Pro+/PPV+ and P1Pro−/P1Pro+ comparisons (adjusted $p < 0.05$). Type ratios of all AS events quantified in the *N. benthamiana* transcriptome analysis, i.e., without applying a p value threshold, are also plotted as a database control (total).

AS genes peaked as early as 1 h and then declined gradually (Supplemental Figure 5B; Supplemental Data 1E). In ABA-dependent responses, the modulation of RNA maturation and diversity thus provides a rapid effect complementary to mechanisms that regulate RNA abundance.

We used a similar bioinformatics workflow to test whether P1Pro infection affects AS and host transcriptomic diversity. An augmented assembly of the *N. benthamiana* transcriptome was generated by merging reported transcriptome datasets (Nakasugi et al., 2014; Kourelis et al., 2019) and transcripts assembled from our RNA-seq data. This augmented transcriptome was used to examine transcript abundance and the diversity of P1Pro or PPV samples from inoculated *N. benthamiana* plants (Supplemental Figure 6). Gene-level differential expression and functional analyses were consistent with and reinforced the findings described above. In the wild-type host, using PPV as a reference (PPV+ samples), P1Pro infection significantly altered host expression profiles, which were again dominated by the up-regulation of genes functionally related to defense response, SA and ABA signaling, and protein phosphorylation (Supplemental Figure 6A–6C; Supplemental Data 1F). Transcriptomic comparison of PPV+ and P1Pro+ samples and P1Pro-inoculated *N. benthamiana nahG* plants (P1Pro−) revealed a comprehensive list of 84 genes whose regulation was altered by P1Pro independent of SA signaling (i.e., SA-independent genes; Supplemental Figure 6A and 6D; Supplemental Data 1G). This SA-independent gene list comprised homologs of known *A. thaliana* ABA-responsive genes and validated the previous identification of *OZF1* and *AGO2* (Supplemental

Figure 6D). Information from quantified transcripts was then used to identify splice events that were differentially regulated by P1Pro infection (Supplemental Data 1H). By comparing P1Pro and PPV samples from wild-type plants (P1Pro+/PPV+), 156 AS events classified as SE, RI, MX, A5, and A3 were identified with an adjusted p value of < 0.05 (Supplemental Figure 6E). Among these AS types, RI was predominant, and its frequency in the differential AS events was higher (51%; $p < 0.05$ set) than that of a reference list composed of all events quantified in the P1Pro+/PPV+ comparison (45%; Total set).

P1Pro infection triggers ABA accumulation (Figure 3A), and an unsupervised multivariate analysis was used to assess similarities between AS linked to P1Pro infection and AS linked to ABA (Figure 4F). The representation of principal components showed that the distributions of AS types identified in the P1Pro+/PPV+ or time series ABA/mock comparisons were grouped and were unrelated to those associated with host genotype (P1Pro−/P1Pro+ comparison) or to a bias of the reference transcriptomic dataset. Hierarchical clustering and bootstrap analysis corroborated the association of AS differentially regulated by ABA or P1Pro (Supplemental Figure 6F). These results strongly suggest that AS triggered by P1Pro is biologically relevant; thus, P1Pro infection has a broad impact on the plant transcriptome by simultaneously affecting host RNA abundance and diversity.

Host Genetic ABA Hypersensitivity and RNA Metabolic Perturbation Promote Potyvirus Resistance

PPV was used in a screen of *A. thaliana* mutant lines of core ABA signaling components to test whether genetic perturbation of ABA signaling can alter plant susceptibility to virus infection (Supplemental Figure 7A). Mutant lines of the nuclear cap-binding complex components ABA HYPERSENSITIVE1/CAP BINDING PROTEIN 80 (ABH1/CBP80) and CAP BINDING PROTEIN 20 (CBP20) were also analyzed (Hugouvieux et al., 2001; Papp et al., 2004). ABA had no effect on *CBP20* or *CBP80* expression (Supplemental Figure 5C), however, CBP20 phosphorylation was altered by the ABA treatment or osmotic stress (Figure 4D). Deficiencies in the nuclear cap-binding complex cause ABA hypersensitivity and broad RNA metabolic defects but have no known effect on antiviral RNA silencing (Daszkowska-Golec, 2018; Kørner et al., 2018). Following PPV agro-inoculation, ABA-hyposensitive lines showed no obvious differences in virus accumulation, possibly due to genetic redundancy (Supplemental Figure 7A). By contrast, ABA-hypersensitive lines showed reduced virus accumulation as assessed by immunoblot analysis of the PPV coat protein (CP). Time course infection analysis showed that PPV levels were significantly lower in *abh1(cbp80)* and *cbp20* lines than in wild-type plants at 10 days post-agroinoculation (dpa), and PPV amounts increased at later times (Figure 5A and Supplemental Figure 7B). The results suggest that cap-binding complex mutants are susceptible hosts in which the onset of PPV infection is significantly delayed.

We evaluated the role of the cap-binding complex in *N. benthamiana* by virus-induced gene silencing (VIGS) of the *NbCBP80* and *NbCBP20* homologs, using the pTRV2-cbp80 or the pTRV2-cbp20 constructs, respectively; gene knockdown was confirmed by qRT–PCR assays (Figure 5B). PPV was inoculated mechanically to avoid possible confounding effects of *Agrobacterium*. At 6 dpi, fluorescence imaging of the viral reporter GFP showed a clear signal in upper uninoculated leaves of control plants, whereas GFP fluorescence was barely detectable in pTRV2-cbp20 or pTRV2-cbp80 conditions (Figure 5C). Immunoblotting confirmed that PPV accumulation was significantly reduced in pTRV2-cbp20 and pTRV2-cbp80 samples ($p < 0.01$, Figure 5D and Supplemental Figure 7C). In agreement with the mRNA quantification, immunoblotting with anti-CBP20 antibodies showed that the signal of a major band in control samples dropped in pTRV2-cbp20 samples ($p = 0.001$, Supplemental Figure 7C). In *A. thaliana*, the CBP20 protein is stabilized by CBP80, and its accumulation is impaired in the *abh1*(*cbp80*) mutant line (Daszkowska-Golec, 2018). Consistent with this finding, anti-CBP20 immunoblotting showed that the major CBP20 band could not be detected in either pTRV2-cbp20 or pTRV2-cbp80 samples (Figure 5D). The collective results of *A. thaliana* and *N. benthamiana* assays indicate that defects in the nuclear cap-binding complex promote plant resistance to PPV.

ABA Treatment Enhances Potyvirus Resistance

To provide additional evidence of ABA antiviral effects, we treated PPV-inoculated *N. benthamiana* plants with control (DMSO) or ABA solutions (50 or 25 μM). At 6 dpi, upper uninoculated leaves of control plants showed a clear signal for the viral reporter GFP, whereas GFP fluorescence was barely detectable in ABA-treated plants (Figure 5E). CP immunoblotting confirmed significantly reduced PPV accumulation in plant samples treated with ABA solutions compared with controls (Figure 5E and Supplemental Figure 7D). The results in Figures 3 and 5 thus indicate that the self-controlled PPV prevents or limits the activation of ABA signaling, which in turn promotes antiviral immunity once activated by a genetic or exogenous means.

In Silico Simulations Support Controlled Polyprotein Processing as an Enhancement Mechanism for Virus Accumulation

Host RNA-silencing and hormone-mediated defenses, as well as self-controlled processing of viral polyproteins, were integrated into a mathematical model to assess their contributions to potyvirus fitness (Figure 6A). We developed a model based on four ordinary differential equations, which included the viral RNA, the viral polyprotein and processed proteins, and host antiviral immunity mediated by RNA silencing and hormone signaling as variables (Supplemental Table 3). In the wild-type virus scenario, polyprotein processing was assumed to depend on a host factor (*H*) that, in a finite, limiting amount, relieves the autoinhibition of P1 cleavage and HCPro release (i.e., self-controlled virus; Figure 6A, top; WT, Supplemental Figure 8). The conditional, controlled release of viral proteins reduced the effectiveness of silencing suppression and the viral amplification rate but allowed the evasion of hormone-mediated defenses and high viral loads at later times. In the second scenario, uncontrolled self-cleavage was simulated in the limit of infinite *H* amount (Figure 6A, bottom; P1Pro, Supplemental Figure 8). Unrestricted, continuous polyprotein processing promoted high viral loads but also the activation of defense response at early times; these were followed by a drop in viral load at later times.

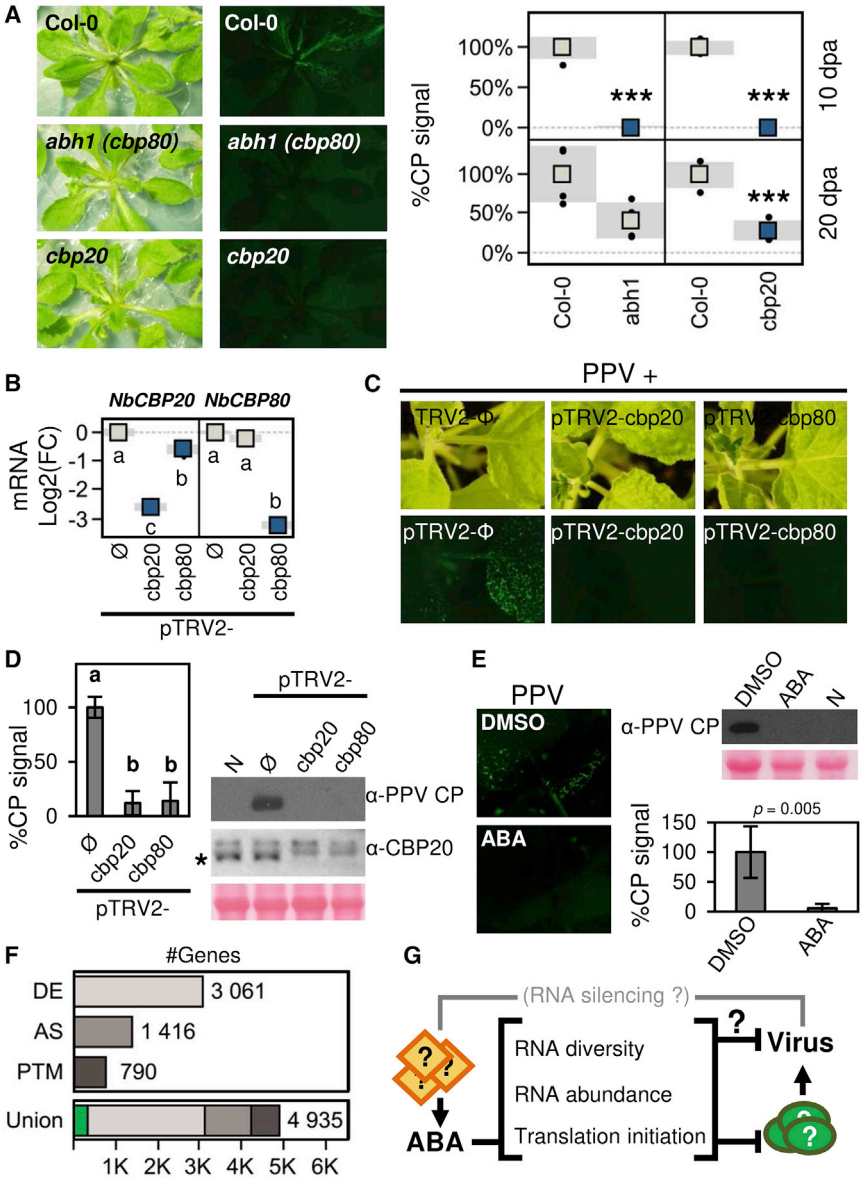

Figure 5. ABA and the Perturbation of Host RNA Metabolism Promote Plant Resistance to PPV Infection.

(A) Genetic depletion of cap-binding complex promotes PPV resistance. Images show green fluorescence in *A. thaliana abh1*(*cbp80*) and *cbp20* lines inoculated with the GFP-tagged PPV. At the indicated dpa, virus accumulation was assessed by anti-PPV coat protein (CP) immunoblots. CP signal values are plotted (mean ± SD, $n = 4$); ***$p < 0.001$ by Student's *t*-test.

(B–D) Silencing of cap-binding complex genes reduces PPV accumulation in *N. benthamiana*. The pTRV2-cbp20 or pTRV2-cbp80 VIGS vectors were delivered to target *NbCBP20* and *NbCBP80* transcripts, respectively; pTRV2-Φ, empty vector control. In **(B)**, the plots of endogenous transcript quantification show mean ± SD (boxes and shadows, respectively; $n = 4$); letters indicate $p < 0.01$, one-way ANOVA and Tukey's HSD test. TRV-treated plants were inoculated with GFP-tagged PPV, and samples were collected from upper uninoculated leaves after 6 days; green fluorescence images are shown in **(C)**. **(D)** Immunoblots show the accumulation of virus (anti-PPV CP) and CBP20. The asterisk marks a major band detected using the anti-CBP20 serum. This band is absent from pTRV2-cbp20 and pTRV2-cbp80 samples. N, untreated sample. The bar plot shows CP signal values (mean ± SD, $n = 4$); letters indicate $p < 0.01$, one-way ANOVA and Tukey's HSD test.

(E) ABA treatments delay PPV infection. Plants were mechanically inoculated with the GFP-tagged PPV and treated with 25 μM ABA or a mock solution (DMSO). Green fluorescence images were taken and samples for immunoblot analysis were collected from upper uninoculated leaves at 6 dpi. Anti-PPV CP immunoblot and signal quantification values are shown (mean ± SD, $n = 4$); p value is shown (Student's *t*-test). Ponceau red-stained blots are shown as a loading control.

(F) Genome-wide impact of ABA. The plot shows *A. thaliana* genes differentially expressed (DE), alternatively spliced (AS), or post-translationally regulated (PTM) by ABA, as identified in Supplemental Figure 5C and Figure 4A. The cumulative number of regulated genes and their overlap (green) are shown at the bottom (see Supplemental Data 1E).

(G) A regulatory model of ABA and RNA metabolic pathways in antiviral immunity. Modulation of RNA diversity, abundance, and turnover and translation initiation by ABA signaling could impair host factors with pro-viral functions or directly act on host or viral components to promote plant resistance. Perturbation of RNA silencing may be involved in ABA activation during virus infection.

In the model, uncontrolled self-cleavage triggers defense activation through the enhancement of silencing suppression and viral amplification rates. The effect of viral replication itself on the activation of defense response were explored by varying the RNA synthesis rate (k_{syn}) or RNA binding constant (θ) parameters of the viral replicase (Supplemental Figure 9). Simulations showed that the θ value has negligible effects on viral replication dynamics (Supplemental Figure 9A). By contrast, an increase in RNA synthesis rate triggered a rapid viral amplification and defense response activation, followed by a drop in viral load at later times (Supplemental Figure 9B and 9C). These results mimicked those of the uncontrolled self-cleavage simulation, albeit to a lesser extent due to the preservation of controlled polyprotein processing. Although oversimplified, this pathosystem model supports the controlled processing of viral polyproteins as a regulatory mechanism for virus accumulation that defines the timing and magnitude of host defense response activation and, consequently, the pathogen fitness.

A Working Model to Explain P1 Variability in the *Potyviridae*

P1 self-cleavage requirements vary greatly in the *Potyviridae* family; in addition, some potyvirids lack P1, and thus its control function over the viral silencing suppressor (Cui and Wang, 2019). We

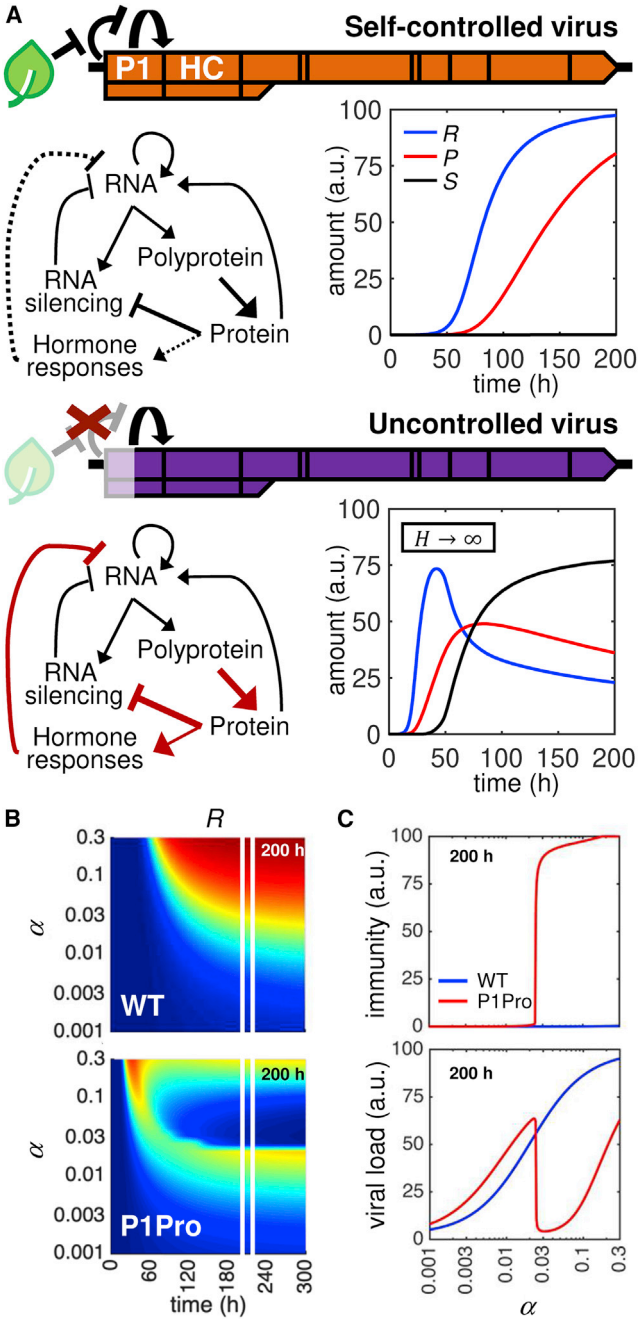

Figure 6. Mathematical Model of Within-Host Viral Replication—Interplay between Viral Polyprotein Processing and Host RNA Silencing and Hormone Responses.

(A) A mathematical model was developed and the numerical simulations of viral RNA (*R*, blue line), mature protein (*P*, red), and immune response (*S*, black) levels are shown for different scenarios. Top, the autoinhibition of P1 self-cleavage and HCPro release is relieved by a host cofactor (*H*) at a finite, limiting amount. The controlled release of HCPro, an RNA-silencing suppressor, allows the attenuation of pathogen virulence and the evasion of hormone-mediated defense responses. This regulatory mechanism assures high long-term viral loads. Bottom, removal of the P1 autoinhibitory domain (simulated with $H \rightarrow \infty$) leads to an uncontrolled release of HCPro and the suppression of RNA silencing but activates hormone responses that restrict viral amplification.

(B) Time course simulations for varying strength of the RNA-silencing suppression (α). Viral RNA (*R*) accumulation relative to the maximum (dark blue for 0% and dark red for 100%) is shown for the wild-type PPV (WT, top) and the uncontrolled self-cleavage (P1Pro, bottom) scenarios. The 200-h time point is marked and plotted in **(C)**.

(C) Viral RNA load (bottom) and immune response (top) levels at 200 h of the dynamics shown in **(B)**. The wild-type PPV (WT, blue) and the uncontrolled self-cleavage (P1Pro, red) scenarios are shown; α, strength of the RNA-silencing suppression.

tested whether the adjustment of silencing suppressor activity would itself be sufficient to compensate for the lack of controlled P1 self-cleavage. The effects of varying the strength of RNA-silencing suppression (α) on infection dynamics were explored with (WT) or without (P1Pro) controlled polyprotein processing. Simulations of viral RNA (*R*) accumulation showed that a low α value enhances P1Pro loads (in our model, $\alpha \sim 0.01$; Figure 6B). A reduction in RNA-silencing suppression strength permitted P1Pro to avoid the activation of immune responses and to outperform the wild-type, self-controlled virus in terms of accumulation ($\alpha < 0.02$; Figure 6C and Supplemental Figure 10). In other words, the acquisition of mutations that reduce suppression strength is predicted to be sufficient to escape hormone-mediated defenses and overcome the lack of P1 or self-cleavage control. These results suggest that uncontrolled self-cleavage (or P1 absence) would be advantageous in hosts with stringent RNA silencing or in which the virus replicates deficiently; conversely, the regulation of P1 cleavage and silencing suppressor activity would maximize viral fitness in adapted hosts.

DISCUSSION

Viruses are obligate parasites that, to maximize their fitness, must evolve control mechanisms to escape host immunity, while simultaneously avoiding acute responses that might lead to early host death. We previously identified an autoinhibitory domain in PPV that controls P1 self-cleavage, which in turn modulates the release of a functional RNA-silencing suppressor and viral replication (Pasin et al., 2014).

Here, a genome-wide analysis showed that P1Pro, a PPV clone that lacks the P1 autoinhibitory domain, triggered complex transcriptomic changes that included the SA and possibly the pipecolate pathways, central components of plant systemic acquired resistance and antiviral immunity (Hartmann and Zeier, 2019; Wang et al., 2019; Murphy et al., 2020). Infection of SA signaling-defective hosts led to the identification of additional players in P1Pro-induced responses, and meta-analysis using our transcriptomic datasets and those of hormone-treated *A. thaliana* plants highlighted the contribution of ABA. Our findings here indicate that multiple host signals, such as SA, ABA, and (possibly) pipecolate, overlap to provide robust defense responses to P1Pro, which are evaded by the wild-type PPV.

The P1Pro infections showed HR accompanied by an increase in ABA levels and the expression of *OZF1*, which encodes an ABA-responsive transcription factor thought to participate in PTI/ETI (Lee et al., 2012; Cao et al., 2019). How can P1Pro infection trigger ABA-dependent responses? Various viral components, such as viral nucleic acids, proteins, and their activities, can act as pathogenesis determinants and elicit ETI (García and Pallás, 2015). In our assays, the truncated P1 version that lacks the

autoinhibitory domain and is encoded by the P1Pro clone was itself insufficient to elicit local HR. This indicates that additional factors of P1Pro infection contribute to systemic ETI, which is inactive during infection with wild-type PPV, including the full-length, self-controlled P1. A single mutation of the polymerase domain of *Plantago asiatica* mosaic virus was shown to promote viral replication, and the resultant necrotic symptoms were caused by overaccumulation of an elicitor domain located in the viral helicase domain (Komatsu et al., 2011). Uncontrolled infection may also lead to autoimmune responses due to the activation of otherwise silent host components. Excess silencing suppression could cause disease by relieving microRNA repression of resistance genes (Li et al., 2012; Shivaprasad et al., 2012) or by altering the biogenesis of virus-activated small interfering RNAs (Cao et al., 2014).

Several lines of evidence indicate that RNA silencing and ABA signaling are interlinked, and ABA was found to affect the transcript level of RNA-silencing genes, as recently reviewed by Alazem and Lin (2020). Despite this body of data, our meta-analysis of available microarray and RNA-seq datasets revealed that the main RNA-silencing genes are unlikely to be primary transcriptional targets of ABA signaling. Treatment of 10 μM ABA was sufficient to upregulate the expression of known ABA marker genes in *A. thaliana* seedlings (Nemhauser et al., 2006; Song et al., 2016); by contrast, the transcript levels of RNA-silencing genes were largely unaffected. These discrepancies might be explained by differences in the amount and timing of phytohormone treatments or by plant growth stages, which were recently shown to influence ABA perception (Berens et al., 2019). Differences in experimental and technical focus and setups should also be considered. Transcriptome-wide microarray or RNA-seq analyses might provide a more accurate, unbiased estimate of transcript abundance than qRT–PCR. In this regard, the expression of host genes commonly used as references in qRT–PCR assays might fluctuate after ABA treatment (e.g., *ACT2* or *ACT8*; Supplemental Figure 5C) and interfere with the quantification of targeted transcripts.

AGO2 is a main RNA-silencing component for plant resistance to RNA viruses (Carbonell and Carrington, 2015). AGO2 and ABA were found to accumulate differentially in P1Pro versus PPV infections. In our assays, AGO2 genetic depletion was itself insufficient to induce ABA in control conditions or to prevent ABA and SA accumulation during P1Pro infection. A recombinant PVX clone with high silencing suppressor activity was shown to induce ABA (Pacheco et al., 2012). Here, in a complementary approach, PVX infection of the *ago2* mutant line was characterized by significantly augmented ABA levels. In contrast to P1Pro or PVX infection results, the PPV clone with a controlled P1 self-cleavage and silencing suppressor release could avoid ABA induction in the wild-type or RNA-silencing-defective hosts.

Viral silencing suppressors are known to target endogenous factors that regulate antiviral RNA silencing and cell RNA metabolism and to affect viral fitness and the transcriptomic profiles of infected hosts (Cervera et al., 2018; Valli et al., 2018; Li and Wang, 2019). One intriguing possibility is that an excess of silencing suppression and viral replication or translation products prime ABA signaling directly or as a result of cellular metabolic/ionic homeostasis perturbation or HR. This would safeguard plants against the depletion of antiviral RNA-silencing components and provide an additional layer of immunity. In tobacco, the simultaneous perception of a viral silencing suppressor and unbalanced cellular ionic homeostasis activates HR and SA signaling (Jeon et al., 2017). It would be interesting to determine whether this perception also triggers ABA, which coordinates plant response to osmotic stress.

If ABA signaling does not regulate the transcript abundance of RNA-silencing genes, what is the functional role of ABA in antiviral immunity? A network of protein phosphatases and kinases mediates ABA signaling and plant responses to osmotic stress (Cutler et al., 2010; Umezawa et al., 2013; Wang et al., 2013, 2020), and this network might post-translationally regulate host proteins that are directly or indirectly necessary for plant immunity or susceptibility. Translation inhibition, RNA maturation and turnover, and their regulation by phosphorylation events have critical roles in the antiviral immune responses of human cells (Narayanan and Makino, 2013; McCormick and Khaperskyy, 2017; Boudreault et al., 2019). In plants, phosphorylation events promote RNA decay in response to bacteria and abiotic stress (Xu and Chua, 2012; Soma et al., 2017; Yu et al., 2019), inhibit or disrupt the translation of host transcripts (Bruns et al., 2019; Cho et al., 2019), and have been suggested to alter RNA maturation by affecting the activity or subcellular distribution of splicing factors (Laloum et al., 2018). Consistent with these studies, results of our phosphoproteomic meta-analysis revealed ABA-dependent responsiveness of the phosphorylation status of host components that regulate RNA stability, turnover, maturation, and translation initiation. These included (1) factors known to be needed for potyvirus (eIFiso4G1, but not eIFiso4G2) or potexvirus infection (EXA1) (Nicaise et al., 2007; Yusa et al., 2019); (2) regulators of the emerging antiviral pathway of RNA decay, such as those involved in mRNA decapping (i.e., VCS and VCR) and 5′-3′ mRNA decay (XRN2, XRN3, LARP1A); (3) determinants of mRNA turnover, such as UBP1C, PUM2, PUM4, and TUDOR-SN PROTEIN 2 (TSN2); and (4) components necessary for mRNA splicing, including coilin, a protein recently linked to SA signaling activation in response to virus infection (Mäkinen et al., 2017; Chantarachot and Bailey-Serres, 2018; Li and Wang, 2019; Shaw et al., 2019; Xu et al., 2020).

Although the functional consequences of these phosphorylation events remain to be determined in the context of virus infection, we analyzed alternative splicing of the plant transcriptome, aiming to establish a link between P1Pro-activated responses and ABA-dependent perturbation of RNA metabolism. Alternative splicing is a phenomenon reported in virus (and potyvirus) infection (Martin et al., 2016; Boudreault et al., 2019) and can be used as a proxy for measuring changes in host RNA maturation. Type frequencies of AS events differentially regulated by P1Pro with respect to PPV are similar to those in plant transcriptomes after ABA treatment. This similarity was significantly higher than expected by chance and was unrelated to the AS type frequency of the reference transcriptome used in the analysis, supporting its biological relevance. We anticipate that future use of improved transcriptomic assemblies and high sequencing depths will help better characterize the extent of AS events in *N. benthamiana* infected with P1Pro and other viruses.

Having established links between P1Pro-activated responses, high ABA levels, and ABA-dependent changes in host RNA abundance and diversity, we evaluated the effects of the genetic depletion or downregulation of ABA signaling components on PPV infection. These included components of the nuclear cap-binding complex that were identified in our phosphoproteomic meta-analysis, whose dysregulation is known to cause ABA hypersensitivity and broad RNA metabolic defects (Hugouvieux et al., 2001; Papp et al., 2004; Laubinger et al., 2008; Daszkowska-Golec, 2018). We showed that plant resistance to PPV was enhanced by exogenous ABA application and, in a complementary approach, by the knockout of *CBP20* or *CBP80* in *A. thaliana*, or their downregulation in *N. benthamiana*.

In *A. thaliana*, our analyses showed that ABA signaling affects the transcript abundance, splice dynamics, or protein phosphorylation status of ca. 5000 genes (Figure 5F). Supported by our transcriptomic data, the meta-analysis of *A. thaliana* datasets, and the infection results of hosts defective in the nuclear cap-binding complex, we propose that ABA could promote antiviral immunity through an extensive, multi-level effect on host RNA metabolism (Figure 5G). This would alter the availability of host pro-viral factor or act directly on viral components to promote plant resistance. For effective resistance, protein phosphatases and kinases of the core ABA or downstream pathways might further target and impair the function of host proteins (e.g., translation initiation factors; see above) and viral proteins necessary for virus infection. The phosphorylation of viral proteins regulates viral cell-to-cell movement, suppressor activity, and virion assembly, among other processes (Hung et al., 2014; Hoover et al., 2016; Shen et al., 2018; Zhang et al., 2018; Hervás et al., 2020).

Based on these observations, we built a mathematical model to explain the effect of controlled polyprotein processing on viral replication and the induction of plant defense. The quantitative modeling of a simplified pathosystem and *in silico* simulations corroborated our working hypothesis that controlled viral polyprotein cleavage can act as a key mechanism that maximizes pathogen fitness by balancing viral protein release and replication with the magnitude of RNA silencing and hormone responses. Simulations further showed that a decrease in the strength of silencing suppression could partly compensate for a lack of self-control. Lack of P1 or its uncontrolled self-cleavage described in some potyvirids would therefore be explained by a low replicative capacity that maintains viral accumulation below a threshold needed for the activation of immune responses.

Can P1 or its protease domain have additional, as-yet-undefined roles in potyviral infection? P1 from the tobacco etch virus was shown to bind ribosomal subunits and proposed to stimulate the translation of viral transcripts (Martínez and Daròs, 2014). P1 translation stimulatory activity was not considered in our mathematical modeling because additional experiments are required to determine whether the full-length protein or the protease domain itself (i.e., that encoded by P1Pro) is necessary for P1 interaction with ribosomal subunits and also with polysomal complexes, which include transcripts undergoing active translation (Chantarachot and Bailey-Serres, 2018). According to our working model, P1 self-cleavage regulates viral replication through controlled HCPro release. HCPro was found to localize with RNA turnover components, including the homologs of VCS and UBP1C (Hafrén et al., 2015) and ABA-responsive phosphoproteins identified in our meta-analysis. HCPro interacts physically with and inhibits XRN4 to counteract RNA decay antiviral defense (Li and Wang, 2018). HCPro from the sugarcane mosaic virus is reported to bind host violaxanthin de-epoxidase, an enzyme that regulates ABA precursor abundance (Chen et al., 2017); the importance of this interaction in ABA signaling is currently unknown. Additional HCPro interactions with functionally diverse plant proteins were reviewed by Valli et al. (2018). Controlled P1 self-cleavage could thus fine-tune multiple HCPro functions, including its silencing suppression and RNA decay-antagonizing activities.

Self-control mechanisms have been reported in plant viruses. To attenuate virus accumulation, the tobamovirus movement protein and the sobemovirus P1 promote silencing spread (Vogler et al., 2008; Lacombe et al., 2010), whereas cucumber mosaic virus 2b suppressor activity is antagonized by the viral CP (Zhang et al., 2017). A host-dependent self-control mechanism would allow viruses to sense the status of host physiology and its fluctuations due to environmental factors. The geminivirus-silencing suppressor βC1 was recently shown to activate and be degraded by host autophagy to reduce viral virulence (Ismayil et al., 2020). Cellular peptidylprolyl isomerases or protein chaperones regulate polyprotein cleavage kinetics and the persistence of human and animal viruses, such as the hepatitis C virus, yellow fever virus, and bovine viral diarrhea virus (Kaul et al., 2009; Bozzacco et al., 2016; Isken et al., 2019). More recently, a functional link between polyprotein processing and host RNA metabolism was reported in alphaviruses. Infection by alphaviruses with high polyprotein processing efficiency was found to depend on G3BP, a host regulatory protein involved in RNA translation and turnover (Götte et al., 2020). Such host-dependent regulation of polyprotein cleavage would be especially beneficial for establishing persistent infections that can allow virus adaptation to perennial and long-lived hosts, such as woody trees (Peng et al., 2001; Salvador et al., 2008; Shan et al., 2015, 2018; Su et al., 2016; Kang et al., 2018).

Finally, in human cells, the activation of interferon antiviral immunity results in translation inhibition and the indiscriminate degradation of host and viral RNA by host ribonucleases (Narayanan and Makino, 2013; McCormick and Khaperskyy, 2017). In prokaryotic cells, the activation of a CRISPR/Cas system with nonspecific ribonuclease activity was recently reported to trigger the indiscriminate degradation of host transcripts and provide robust phage immunity through the induction of cellular dormancy (Meeske et al., 2019). In plants, ABA promotes growth arrest and accumulates at high levels in dormant tissues in vegetative organs (Yao and Finlayson, 2015; Martín-Fontecha et al., 2018). The translation initiation disruption and translation repression of a large portion of plant genes were reported in response to dehydration (Kawaguchi et al., 2004), and it is plausible that a similar phenomenon occurs during ABA signaling. ABA-dependent control of host RNA metabolism and translation could contribute to cellular metabolic arrest and dormancy in an antiviral response that shows a striking resemblance to interferon- and CRISPR/Cas-mediated antiviral immunity of human and prokaryotic cells, respectively. ABA may

therefore be an overlooked, active player that controls viral infection dynamics in plants.

MATERIALS AND METHODS

Plant Materials

Wild-type *Nicotiana benthamiana*, the *N. benthamiana nahG*-transgenic line expressing an SA hydroxylase gene (Ying et al., 2010), and the *N. benthamiana ago2* mutant line (Ludman et al., 2017) were grown in a greenhouse with a 16-h light/8-h dark photoperiod in a 19°C–23°C temperature range. The *Arabidopsis thaliana abh1*(*cbp80*) and *cbp20* single-mutant lines (Hugouvieux et al., 2001; Papp et al., 2004) were grown *in vitro* on half-strength Murashige and Skoog medium (pH 5.7) with 2-(N-morpholino)ethanesulfonic acid and vitamins, 1% (w/v) sucrose, and 0.8% (w/v) Bacto Agar and were maintained in a growth chamber (16-h light/8-h dark photoperiod, 21°C ± 1°C, 60% relative humidity).

Plasmids, Virus Inoculation, and VIGS Assays

A full-length cDNA copy of a PPV isolate adapted to *Nicotiana* spp., tagged with a GFP gene, and inserted into the pSN-PPV binary plasmid has been reported (Supplemental Table 4), as has pSN-PPV P1Pro [V164] (herein P1Pro), a pSN-PPV-based vector with a truncated P1 sequence (Pasin et al., 2014). Binary vectors used in transient expression assays were reported or generated as detailed in Supplemental Table 4. A tobacco rattle virus (TRV) system was used to silence endogenous transcripts, and the SGN VIGS tool was used to select suitable regions (Fernandez-Pozo et al., 2015). The assembly of pTRV2-cbp80 and pTRV2-cbp20 and the sequences of the primers and the fragments cloned are detailed in Supplemental Tables 4–7. The *Agrobacterium* C58C1-313 strain (Pasin et al., 2017) was used for plant agro-inoculation and VIGS vector delivery. PPV clones were delivered by *Agrobacterium*-mediated infection to soil- and *in vitro*-grown *N. benthamiana* and *A. thaliana* plants, respectively (Pasin et al., 2014). VIGS assays were conducted as previously described (Aguilar et al., 2019). *Agrobacterium* strains that harbored pTRV1 and pTRV2 or its derivatives were mixed and infiltrated into 2-week-old *N. benthamiana* plants. After 10 days, young plant leaves were inoculated mechanically with PPV. For mechanical inoculations, crude extracts were prepared in 100 mM phosphate buffer (pH 7.2) from agro-infected *N. benthamiana* plants and used as PPV inoculum sources. PPV inoculum was applied with carborundum and gently rubbed on young *N. benthamiana* leaves. PVX was inoculated as previously described (Ludman et al., 2017).

Transcriptomic Analysis

N. benthamiana plants were inoculated by agro-infection (see above), and upper uninoculated leaves were collected at 14 dpa. For each experimental condition, three biological replicates (each sample was a pool of ≥2 infected plants) were used for transcriptomic analysis (RNA-seq). Plant tissues were ground in liquid nitrogen in a mortar, and total RNA was extracted with the FavorPrep plant total RNA mini kit (Favorgen), including on-column DNAse I treatment. Following a second DNAse I digestion, samples were purified by organic extraction and sodium acetate precipitation. Ribosomal RNA molecules were depleted using the RiboMinus plant kit (Invitrogen). Recovered RNA was quantified using a fluorescent RNA binding dye (QuantiFluor RNA system, Promega) and analyzed in a Bioanalyzer with the RNA 6000 Pico kit (Agilent). Libraries were prepared using the TruSeq Stranded mRNA kit (Illumina), omitting the mRNA enrichment step, and were sequenced (2 × 100-nt paired-end reads) on an Illumina HiSeq 2000 platform at the Centro Nacional de Análisis Genómico (CNAG-CRG, Spain) to yield ≥1.8 Gb/sample. See Supplemental Information for details of transcriptomic dataset analysis and gene functional annotations.

A study of hormone-treated *A. thaliana* plants has been reported (Nemhauser et al., 2006), and its microarray data (AT-00110) were obtained from Genevestigator (Hruz et al., 2008). RNA-seq results and transcript fold changes from ABA time series experiments (Song et al., 2016) were retrieved from the NCBI Gene Expression Omnibus (GEO) (GSE80565), and RNA-seq reads were used to analyze AS events (see Supplemental Information).

Quantitative Proteomic and Phosphoproteomic Datasets

Sample preparation, isobaric tag labeling, liquid chromatography-tandem mass spectrometry (LC-MS/MS), and data analysis of *N. benthamiana nahG* plants inoculated with PPV or P1Pro have been described previously (Pasin et al., 2014), and the data are available at ProteomeXchange with identifier PXD017769.

The datasets of *A. thaliana* proteins with significantly altered phosphorylation status in response to ABA or dehydration stress (ABA_DH), ABA (ABA_1, ABA_2), mannitol, or NaCl have been reported (Umezawa et al., 2013; Wang et al., 2013, 2020). Wild-type and *snrk2.2/2.3/2.6* triple-mutant results were considered, and protein lists are included in Supplemental Data 1D. The phosphoproteome from Mergner et al. (2020) was used as a reference list and as the background in GO term enrichment analysis.

qRT–PCR Assays

Total RNA was purified from the upper uninoculated leaf samples using the Plant Total RNA mini kit (Geneaid). To remove DNA contaminants, 1 μg purified RNA was treated with ezDNAse enzyme (Thermo Fisher) before cDNA synthesis using M-MuLV reverse transcriptase (New England BioLabs) and random hexamers. The cDNA samples were used in qPCR reactions that included gene-specific primers (Supplemental Tables 5 and 6) and 5× HOT FIREPol EvaGreen qPCR Mix Plus (Solis BioDyne) and were run on a 7300 real-time PCR System (Applied Biosystems). Expression was normalized using *NbPSMD1* as a reference gene (Supplemental Table 6), and fold changes relative to the control condition were calculated by the $\Delta\Delta^{CT}$ method (Rodamilans et al., 2014) and expressed as log2 values. The RT–PCR assays shown in Figure 4B were performed using the 2174_F/1631_R primers (Supplemental Table 5).

Protein Detection

GFP fluorescence was visualized under an epifluorescence microscope (MZ FLIII, Leica; excitation and emission wavelengths 470/40 and 525/50 nm, respectively) and photographed with an Olympus DP70 digital camera. Total protein extracts from plant samples were prepared and resolved by SDS–PAGE as described previously (Pasin et al., 2014). Immunodetection was conducted using rabbit anti-PPV CP (Pasin et al., 2014) and anti-CBP20 sera (Raczynska et al., 2014) as primary antibodies.

Hormone Quantification and Treatments

Frozen leaf material (~100 mg fresh weight) was extracted in 20:80 (v/v) methanol:isopropanol with 1% glacial acetic acid and isotope-labeled internal standards. Supernatants were analyzed by ultra-performance LC-MS/MS, and free SA and ABA were quantified as described previously (Müller and Munné-Bosch, 2011). For treatment, (±)-ABA (A1049, Sigma) was dissolved in DMSO, and ABA solutions containing 0.005% Silwet-77 were sprayed onto plants once on the day before virus inoculation and twice daily thereafter. A DMSO-containing solution was used as a control. Upper uninoculated leaves were collected at 6 dpi.

Statistics

A two-tailed Student's *t*-test was used for comparisons of two groups. A one-way ANOVA with Tukey's honestly significant difference test was used to assess significant differences between more than two groups. Significance levels of *p* values are indicated in the figures.

Mathematical Modeling

Sigmoidal equations were used to describe different biochemical processes and were then assembled to construct a system of ordinary

differential equations to describe the dynamics (see Supplemental Information). The host was assumed to be a single, uniform compartment in which biochemical processes occurred. Parameter values were chosen according to available experimental data (Supplemental Table 3). Numerical simulations to obtain the dynamic behavior of viral infection were carried out with MATLAB (MathWorks). Different scenarios were modeled by changing key parameter values.

ACCESSION NUMBERS

The RNA-seq raw reads from this study can be found at NCBI under GEO accession number GSE146746 (https://www.ncbi.nlm.nih.gov/geo/query/acc.cgi?acc=GSE146746). Proteomic data from PPV- or P1Pro-inoculated *N. benthamiana* plants are available at the Proteomics Identification Database with identifier PXD017769. The *A. thaliana* microarray datasets from hormone-treated plants are available at Genevestigator (AT-00110). The RNA-seq fold change values and raw reads from ABA time series experiments are available at GEO (GSE80565) and the Sequence Read Archive (SRP073711). Major *A. thaliana* genes mentioned herein are as follows: AGO2, AT1G31280; OZF1, AT2G19810; CBP20, AT5G44200; CBP80, AT2G13540; PP2CA, AT3G11410; SnRK2.2, AT3G50500.

SUPPLEMENTAL INFORMATION

Supplemental Information is available at *Plant Communications Online*.

FUNDING

This work was supported by funds to J.A.G. from the Ministerio de Ciencia e Innovación (Spain), grants BIO2016-80572-R and PID2019-109380RB-I00 / AEI / 10.13039/501100011033 (AEI-FEDER). K.F. is funded by grant K124705 from the National Research Development and Innovation Office (Hungary), and S.M.-B. by grant 2017 SGR 980 from the Generalitat de Catalunya (Spain). Galaxy is a platform supported by NIH grant HG006620. F.P. was the recipient of a post-doctoral fellowship from Academia Sinica (Taiwan).

AUTHOR CONTRIBUTIONS

F.P. and J.A.G. conceived the study. F.P. designed and coordinated the research. F.P., H.S., and B.G. performed the experiments. F.P., D.S.L., and J.A.G. analyzed the data. K.F. and M.L. performed the *N. benthamiana ago2* experiments. S.M.-B., M.M., and D.H.F. carried out the hormone quantification. G.R. developed the mathematical model and performed the numerical simulations. J.A.G., S.M.-B., and K.F. secured funding. F.P. wrote the paper with the collaboration of J.A.G. and G.R. All authors approved the final version of the manuscript.

ACKNOWLEDGMENTS

We are grateful to Bernardo Rodamilans, István Papp, Brian D. Gregory, Eduardo González-Grandío, Pilar Cubas, Francisco Tenllado, Hui-Shan Guo, Gregory B. Martin, Katarzyna Dorota Raczyńska, and Artur Jarmołowski for the supply of materials. We thank Galaxy (Afgan et al., 2018) for computational resources and Catherine Mark for editorial assistance. No conflict of interest declared.

Received: February 20, 2020
Revised: July 3, 2020
Accepted: July 7, 2020
Published: July 7, 2020

REFERENCES

Afgan, E., Baker, D., Batut, B., van den Beek, M., Bouvier, D., Cech, M., Chilton, J., Clements, D., Coraor, N., Grüning, B.A., et al. (2018). The Galaxy platform for accessible, reproducible and collaborative biomedical analyses: 2018 update. Nucleic Acids Res. **46**:W537–W544.

Aguilar, E., Del Toro, F.J., Brosseau, C., Moffett, P., Canto, T., and Tenllado, F. (2019). Cell death triggered by the P25 protein in *Potato virus X*-associated synergisms results from endoplasmic reticulum stress in *Nicotiana benthamiana*. Mol. Plant Pathol. **20**:194–210.

Alazem, M., and Lin, N.-S. (2015). Roles of plant hormones in the regulation of host–virus interactions. Mol. Plant Pathol. **16**:529–540.

Alazem, M., and Lin, N.-S. (2020). Interplay between ABA signaling and RNA silencing in plant viral resistance. Curr. Opin. Virol. **42**:1–7.

Alazem, M., He, M.-H., Moffett, P., and Lin, N.-S. (2017). Abscisic acid induces resistance against *Bamboo mosaic virus* through *Argonaute2* and *3*. Plant Physiol. **174**:339–355.

Berens, M.L., Berry, H.M., Mine, A., Argueso, C.T., and Tsuda, K. (2017). Evolution of hormone signaling networks in plant defense. Annu. Rev. Phytopathol. **55**:401–425.

Berens, M.L., Wolinska, K.W., Spaepen, S., Ziegler, J., Nobori, T., Nair, A., Krüler, V., Winkelmüller, T.M., Wang, Y., Mine, A., et al. (2019). Balancing trade-offs between biotic and abiotic stress responses through leaf age-dependent variation in stress hormone cross-talk. Proc. Natl. Acad. Sci. U S A **116**:2364–2373.

Boudreault, S., Roy, P., Lemay, G., and Bisaillon, M. (2019). Viral modulation of cellular RNA alternative splicing: a new key player in virus-host interactions? Wiley Interdiscip. Rev. RNA **10**:e1543.

Bozzacco, L., Yi, Z., Andreo, U., Conklin, C.R., Li, M.M.H., Rice, C.M., and MacDonald, M.R. (2016). Chaperone-assisted protein folding is critical for yellow fever virus NS3/4A cleavage and replication. J. Virol. **90**:3212–3228.

Bruns, A.N., Li, S., Mohannath, G., and Bisaro, D.M. (2019). Phosphorylation of *Arabidopsis* eIF4E and eIFiso4E by SnRK1 inhibits translation. FEBS J. **286**:3778–3796.

Cao, M., Du, P., Wang, X., Yu, Y.-Q., Qiu, Y.-H., Li, W., Gal-On, A., Zhou, C., Li, Y., and Ding, S.-W. (2014). Virus infection triggers widespread silencing of host genes by a distinct class of endogenous siRNAs in *Arabidopsis*. Proc. Natl. Acad. Sci. U S A **111**:14613–14618.

Cao, F.Y., Khan, M., Taniguchi, M., Mirmiran, A., Moeder, W., Lumba, S., Yoshioka, K., and Desveaux, D. (2019). A host-pathogen interactome uncovers phytopathogenic strategies to manipulate plant ABA responses. Plant J. **100**:187–198.

Carbonell, A., and Carrington, J.C. (2015). Antiviral roles of plant ARGONAUTES. Curr. Opin. Plant Biol. **27**:111–117.

Cervera, H., Ambrós, S., Bernet, G.P., Rodrigo, G., and Elena, S.F. (2018). Viral fitness correlates with the magnitude and direction of the perturbation induced in the host's transcriptome: the tobacco etch potyvirus-tobacco case study. Mol. Biol. Evol. **35**:1599–1615.

Chantarachot, T., and Bailey-Serres, J. (2018). Polysomes, stress granules, and processing bodies: a dynamic triumvirate controlling cytoplasmic mRNA fate and function. Plant Physiol. **176**:254–269.

Chen, L., Zhang, L., Li, D., Wang, F., and Yu, D. (2013). WRKY8 transcription factor functions in the TMV-cg defense response by mediating both abscisic acid and ethylene signaling in *Arabidopsis*. Proc. Natl. Acad. Sci. U S A **110**:1963–1971.

Chen, L., Yan, Z., Xia, Z., Cheng, Y., Jiao, Z., Sun, B., Zhou, T., and Fan, Z. (2017). A violaxanthin deepoxidase interacts with a viral suppressor of RNA silencing to inhibit virus amplification. Plant Physiol. **175**:1774–1794.

Cho, H.-Y., Lu, M.-Y.J., and Shih, M.-C. (2019). The SnRK1-eIFiso4G1 signaling relay regulates the translation of specific mRNAs in *Arabidopsis* under submergence. New Phytol. **222**:366–381.

Cui, H., and Wang, A. (2019). The biological impact of the hypervariable N-terminal region of potyviral genomes. Annu. Rev. Virol. **6**:255–274.

Cutler, S.R., Rodriguez, P.L., Finkelstein, R.R., and Abrams, S.R. (2010). Abscisic acid: emergence of a core signaling network. Annu. Rev. Plant Biol. **61**:651–679.

Daszkowska-Golec, A. (2018). Emerging roles of the nuclear cap-binding complex in abiotic stress responses. Plant Physiol. **176**:242–253.

Fernandez-Pozo, N., Rosli, H.G., Martin, G.B., and Mueller, L.A. (2015). The SGN VIGS tool: user-friendly software to design virus-induced gene silencing (VIGS) constructs for functional genomics. Mol. Plant **8**:486–488.

García, J.A., and Pallás, V. (2015). Viral factors involved in plant pathogenesis. Curr. Opin. Virol. **11**:21–30.

Götte, B., Utt, A., Fragkoudis, R., Merits, A., and McInerney, G.M. (2020). Sensitivity of alphaviruses to G3BP deletion correlates with efficiency of replicase polyprotein processing. J. Virol. **94**, e01681–19.

Hafrén, A., Lõhmus, A., and Mäkinen, K. (2015). Formation of *Potato virus A*-induced RNA granules and viral translation are interrelated processes required for optimal virus accumulation. PLoS Pathog. **11**:e1005314.

Hartmann, M., and Zeier, J. (2019). *N*-hydroxypipecolic acid and salicylic acid: a metabolic duo for systemic acquired resistance. Curr. Opin. Plant Biol. **50**:44–57.

Hervás, M., Navajas, R., Chagoyen, M., García, J.A., and Martínez-Turiño, S. (2020). Phosphorylation-related cross-talk between distant regions of the core region of the coat protein contributes to virion assembly of *Plum pox virus*. Mol. Plant Microbe Interact. **33**:653–667.

Hoover, H.S., Wang, J.C.-Y., Middleton, S., Ni, P., Zlotnick, A., Vaughan, R.C., and Kao, C.C. (2016). Phosphorylation of the brome mosaic virus capsid regulates the timing of viral infection. J. Virol. **90**:7748–7760.

Hruz, T., Laule, O., Szabo, G., Wessendorp, F., Bleuler, S., Oertle, L., Widmayer, P., Gruissem, W., and Zimmermann, P. (2008). Genevestigator v3: a reference expression database for the meta-analysis of transcriptomes. Adv. Bioinformatics **2008**:420747.

Hugouvieux, V., Kwak, J.M., and Schroeder, J.I. (2001). An mRNA cap binding protein, ABH1, modulates early abscisic acid signal transduction in *Arabidopsis*. Cell **106**:477–487.

Hung, C.-J., Huang, Y.-W., Liou, M.-R., Lee, Y.-C., Lin, N.-S., Meng, M., Tsai, C.-H., Hu, C.-C., and Hsu, Y.-H. (2014). Phosphorylation of coat protein by protein kinase CK2 regulates cell-to-cell movement of *Bamboo mosaic virus* through modulating RNA binding. Mol. Plant Microbe Interact. **27**:1211–1225.

Isken, O., Postel, A., Bruhn, B., Lattwein, E., Becher, P., and Tautz, N. (2019). CRISPR/Cas9-mediated knockout of DNAJC14 verifies this chaperone as a pivotal host factor for RNA replication of pestiviruses. J. Virol. **93**:e01714–e01718.

Ismayil, A., Yang, M., Haxim, Y., Wang, Y., Li, J., Han, L., Wang, Y., Zheng, X., Wei, X., Nagalakshmi, U., et al. (2020). *Cotton leaf curl Multan virus* βC1 protein induces autophagy by disrupting the interaction of autophagy-related protein 3 with glyceraldehyde-3-phosphate dehydrogenases. Plant Cell **32**:1124–1135.

Jeon, E.J., Tadamura, K., Murakami, T., Inaba, J.-I., Kim, B.M., Sato, M., Atsumi, G., Kuchitsu, K., Masuta, C., and Nakahara, K.S. (2017). rgs-CaM detects and counteracts viral RNA silencing suppressors in plant immune priming. J. Virol. **91**, e00761–17.

Kang, S.-H., Atallah, O.O., Sun, Y.-D., and Folimonova, S.Y. (2018). Functional diversification upon leader protease domain duplication in the *Citrus tristeza virus* genome: role of RNA sequences and the encoded proteins. Virology **514**:192–202.

Kaul, A., Stauffer, S., Berger, C., Pertel, T., Schmitt, J., Kallis, S., Zayas, M., Lopez, M.Z., Lohmann, V., Luban, J., et al. (2009). Essential role of cyclophilin A for hepatitis C virus replication and virus production and possible link to polyprotein cleavage kinetics. PLoS Pathog. **5**:e1000546.

Kawa, D., and Testerink, C. (2017). Regulation of mRNA decay in plant responses to salt and osmotic stress. Cell. Mol. Life Sci. **74**:1165–1176.

Kawaguchi, R., Girke, T., Bray, E.A., and Bailey-Serres, J. (2004). Differential mRNA translation contributes to gene regulation under non-stress and dehydration stress conditions in *Arabidopsis thaliana*. Plant J. **38**:823–839.

Komatsu, K., Hashimoto, M., Maejima, K., Shiraishi, T., Neriya, Y., Miura, C., Minato, N., Okano, Y., Sugawara, K., Yamaji, Y., et al. (2011). A necrosis-inducing elicitor domain encoded by both symptomatic and asymptomatic *Plantago asiatica mosaic virus* isolates, whose expression is modulated by virus replication. Mol. Plant Microbe Interact. **24**:408–420.

Kørner, C.J., Pitzalis, N., Peña, E.J., Erhardt, M., Vazquez, F., and Heinlein, M. (2018). Crosstalk between PTGS and TGS pathways in natural antiviral immunity and disease recovery. Nat. Plants **4**:157–164.

Kourelis, J., Kaschani, F., Grosse-Holz, F.M., Homma, F., Kaiser, M., and van der Hoorn, R.A.L. (2019). A homology-guided, genome-based proteome for improved proteomics in the alloploid *Nicotiana benthamiana*. BMC Genomics **20**:722.

Lackner, T., Müller, A., Pankraz, A., Becher, P., Thiel, H.-J., Gorbalenya, A.E., and Tautz, N. (2004). Temporal modulation of an autoprotease is crucial for replication and pathogenicity of an RNA virus. J. Virol. **78**:10765–10775.

Lacombe, S., Bangratz, M., Vignols, F., and Brugidou, C. (2010). The rice yellow mottle virus P1 protein exhibits dual functions to suppress and activate gene silencing. Plant J. **61**:371–382.

Laloum, T., Martín, G., and Duque, P. (2018). Alternative splicing control of abiotic stress responses. Trends Plant Sci. **23**:140–150.

Laubinger, S., Sachsenberg, T., Zeller, G., Busch, W., Lohmann, J.U., Ratsch, G., and Weigel, D. (2008). Dual roles of the nuclear cap-binding complex and SERRATE in pre-mRNA splicing and microRNA processing in *Arabidopsis thaliana*. Proc. Natl. Acad. Sci. U S A **105**:8795–8800.

Lee, S., Jung, H.J., Kang, H., and Kim, S.Y. (2012). *Arabidopsis* zinc finger proteins AtC3H49/AtTZF3 and AtC3H20/AtTZF2 are involved in ABA and JA responses. Plant Cell Physiol. **53**:673–686.

Lei, J., and Hilgenfeld, R. (2017). RNA-virus proteases counteracting host innate immunity. FEBS Lett. **591**:3190–3210.

Li, F., and Wang, A. (2018). RNA decay is an antiviral defense in plants that is counteracted by viral RNA silencing suppressors. PLoS Pathog. **14**:e1007228.

Li, F., and Wang, A. (2019). RNA-targeted antiviral immunity: more than just RNA silencing. Trends Microbiol. **27**:792–805.

Li, F., Pignatta, D., Bendix, C., Brunkard, J.O., Cohn, M.M., Tung, J., Sun, H., Kumar, P., and Baker, B. (2012). MicroRNA regulation of plant innate immune receptors. Proc. Natl. Acad. Sci. U S A **109**:1790–1795.

Ludman, M., Burgyán, J., and Fátyol, K. (2017). CRISPR/Cas9 mediated inactivation of Argonaute 2 reveals its differential involvement in antiviral responses. Sci. Rep. **7**:1010.

Mäkinen, K., Lõhmus, A., and Pollari, M. (2017). Plant RNA regulatory network and RNA granules in virus infection. Front. Plant Sci. **8**:2093.

Mann, K., and Sanfaçon, H. (2019). Expanding repertoire of plant positive-strand RNA virus proteases. Viruses **11**:66.

Martin, K., Singh, J., Hill, J.H., Whitham, S.A., and Cannon, S.B. (2016). Dynamic transcriptome profiling of bean common mosaic virus (BCMV) infection in common bean (*Phaseolus vulgaris* L.). BMC Genomics **17**:613.

Martínez, F., and Daròs, J.-A. (2014). *Tobacco etch virus* protein P1 traffics to the nucleolus and associates with the host 60S ribosomal subunits during infection. J. Virol. **88**:10725–10737.

Martínez, F., Rodrigo, G., Aragonés, V., Ruiz, M., Lodewijk, I., Fernández, U., Elena, S.F., and Daròs, J.-A. (2016). Interaction network of tobacco etch potyvirus NIa protein with the host proteome during infection. BMC Genomics **17**:87.

Martín-Fontecha, E.S., Tarancón, C., and Cubas, P. (2018). To grow or not to grow, a power-saving program induced in dormant buds. Curr. Opin. Plant Biol. **41**:102–109.

McCormick, C., and Khaperskyy, D.A. (2017). Translation inhibition and stress granules in the antiviral immune response. Nat. Rev. Immunol. **17**:647–660.

Meeske, A.J., Nakandakari-Higa, S., and Marraffini, L.A. (2019). Cas13-induced cellular dormancy prevents the rise of CRISPR-resistant bacteriophage. Nature **570**:241–245.

Mergner, J., Frejno, M., List, M., Papacek, M., Chen, X., Chaudhary, A., Samaras, P., Richter, S., Shikata, H., Messerer, M., et al. (2020). Mass-spectrometry-based draft of the *Arabidopsis* proteome. Nature **579**:409–414.

Müller, M., and Munné-Bosch, S. (2011). Rapid and sensitive hormonal profiling of complex plant samples by liquid chromatography coupled to electrospray ionization tandem mass spectrometry. Plant Methods **7**:37.

Murphy, A.M., Zhou, T., and Carr, J.P. (2020). An update on salicylic acid biosynthesis, its induction and potential exploitation by plant viruses. Curr. Opin. Virol. **42**:8–17.

Nakahara, K.S., and Masuta, C. (2014). Interaction between viral RNA silencing suppressors and host factors in plant immunity. Curr. Opin. Plant Biol. **20**:88–95.

Nakasugi, K., Crowhurst, R., Bally, J., and Waterhouse, P. (2014). Combining transcriptome assemblies from multiple *de novo* assemblers in the allo-tetraploid plant *Nicotiana benthamiana*. PLoS One **9**:e91776.

Narayanan, K., and Makino, S. (2013). Interplay between viruses and host mRNA degradation. Biochim. Biophys. Acta **1829**:732–741.

Nemhauser, J.L., Hong, F., and Chory, J. (2006). Different plant hormones regulate similar processes through largely nonoverlapping transcriptional responses. Cell **126**:467–475.

Nicaise, V., Gallois, J.-L., Chafiai, F., Allen, L.M., Schurdi-Levraud, V., Browning, K.S., Candresse, T., Caranta, C., Le Gall, O., and German-Retana, S. (2007). Coordinated and selective recruitment of eIF4E and eIF4G factors for potyvirus infection in *Arabidopsis thaliana*. FEBS Lett. **581**:1041–1046.

Nobori, T., Mine, A., and Tsuda, K. (2018). Molecular networks in plant-pathogen holobiont. FEBS Lett. **592**:1937–1953.

Pacheco, R., García-Marcos, A., Manzano, A., de Lacoba, M.G., Camañes, G., García-Agustín, P., Díaz-Ruíz, J.R., and Tenllado, F. (2012). Comparative analysis of transcriptomic and hormonal responses to compatible and incompatible plant-virus interactions that lead to cell death. Mol. Plant Microbe Interact. **25**:709–723.

Papp, I., Mur, L.A., Dalmadi, A., Dulai, S., and Koncz, C. (2004). A mutation in the *Cap Binding Protein 20* gene confers drought tolerance to *Arabidopsis*. Plant Mol. Biol. **55**:679–686.

Pasin, F., Simón-Mateo, C., and García, J.A. (2014). The hypervariable amino-terminus of P1 protease modulates potyviral replication and host defense responses. PLoS Pathog. **10**:e1003985.

Pasin, F., Bedoya, L.C., Bernabé-Orts, J.M., Gallo, A., Simón-Mateo, C., Orzaez, D., and García, J.A. (2017). Multiple T-DNA delivery to plants using novel mini binary vectors with compatible replication origins. ACS Synth. Biol. **6**:1962–1968.

Pasin, F., Menzel, W., and Daròs, J.-A. (2019). Harnessed viruses in the age of metagenomics and synthetic biology: an update on infectious clone assembly and biotechnologies of plant viruses. Plant Biotechnol. J. **17**:1010–1026.

Paudel, D.B., and Sanfaçon, H. (2018). Exploring the diversity of mechanisms associated with plant tolerance to virus infection. Front. Plant Sci. **9**:1575.

Peng, C.-W., Peremyslov, V.V., Mushegian, A.R., Dawson, W.O., and Dolja, V.V. (2001). Functional specialization and evolution of leader proteinases in the family *Closteroviridae*. J. Virol. **75**:12153–12160.

Raczynska, K.D., Stepien, A., Kierzkowski, D., Kalak, M., Bajczyk, M., McNicol, J., Simpson, C.G., Szweykowska-Kulinska, Z., Brown, J.W.S., and Jarmolowski, A. (2014). The SERRATE protein is involved in alternative splicing in *Arabidopsis thaliana*. Nucleic Acids Res. **42**:1224–1244.

Revers, F., and García, J.A. (2015). Molecular biology of potyviruses. Adv. Virus Res. **92**:101–199.

Rodamilans, B., San León, D., Mühlberger, L., Candresse, T., Neumüller, M., Oliveros, J.C., and García, J.A. (2014). Transcriptomic analysis of *Prunus domestica* undergoing hypersensitive response to *Plum pox virus* infection. PLoS One **9**:e100477.

Rodamilans, B., Shan, H., Pasin, F., and García, J.A. (2018). Plant viral proteases: beyond the role of peptide cutters. Front. Plant Sci. **9**:666.

Salvador, B., Saénz, P., Yangüez, E., Quiot, J.B., Quiot, L., Delgadillo, M.O., García, J.A., and Simón-Mateo, C. (2008). Host-specific effect of P1 exchange between two potyviruses. Mol. Plant Pathol. **9**:147–155.

Seo, J.-K., Kwon, S.-J., Cho, W.K., Choi, H.-S., and Kim, K.-H. (2014). Type 2C protein phosphatase is a key regulator of antiviral extreme resistance limiting virus spread. Sci. Rep. **4**:5905.

Shan, H., Pasin, F., Valli, A., Castillo, C., Rajulu, C., Carbonell, A., Simón-Mateo, C., García, J.A., and Rodamilans, B. (2015). The *Potyviridae* P1a leader protease contributes to host range specificity. Virology **476**:264–270.

Shan, H., Pasin, F., Tzanetakis, I.E., Simón-Mateo, C., García, J.A., and Rodamilans, B. (2018). Truncation of a P1 leader proteinase facilitates potyvirus replication in a non-permissive host. Mol. Plant Pathol. **19**:1504–1510.

Shaw, J., Yu, C., Makhotenko, A.V., Makarova, S.S., Love, A.J., Kalinina, N.O., MacFarlane, S., Chen, J., and Taliansky, M.E. (2019). Interaction of a plant virus protein with the signature Cajal body protein coilin facilitates salicylic acid-mediated plant defence responses. New Phytol. **224**:439–453.

Shen, W., Bobay, B.G., Greeley, L.A., Reyes, M.I., Rajabu, C.A., Blackburn, R.K., Dallas, M.B., Goshe, M.B., Ascencio-Ibáñez, J.T., and Hanley-Bowdoin, L. (2018). Sucrose nonfermenting 1-related protein kinase 1 phosphorylates a geminivirus Rep protein to impair viral replication and infection. Plant Physiol. **178**:372–389.

Shen, W., Shi, Y., Dai, Z., and Wang, A. (2020). The RNA-dependent RNA polymerase NIb of potyviruses plays multifunctional, contrasting roles during viral infection. Viruses **12**:77.

Shivaprasad, P.V., Chen, H.-M., Patel, K., Bond, D.M., Santos, B.A.C.M., and Baulcombe, D.C. (2012). A microRNA superfamily regulates nucleotide binding site-leucine-rich repeats and other mRNAs. Plant Cell **24**:859–874.

Soma, F., Mogami, J., Yoshida, T., Abekura, M., Takahashi, F., Kidokoro, S., Mizoi, J., Shinozaki, K., and Yamaguchi-Shinozaki, K. (2017). ABA-unresponsive SnRK2 protein kinases regulate mRNA decay under osmotic stress in plants. Nat. Plants **3**:16204.

Song, L., Huang, S.-S.C., Wise, A., Castanon, R., Nery, J.R., Chen, H., Watanabe, M., Thomas, J., Bar-Joseph, Z., and Ecker, J.R. (2016). A transcription factor hierarchy defines an environmental stress response network. Science **354**:aag1550.

Su, X., Fu, S., Qian, Y., Zhang, L., Xu, Y., and Zhou, X. (2016). Discovery and small RNA profile of *Pecan mosaic-associated virus*, a novel potyvirus of pecan trees. Sci. Rep. **6**:26741.

Tsuda, K., and Somssich, I.E. (2015). Transcriptional networks in plant immunity. New Phytol. **206**:932–947.

Umezawa, T., Sugiyama, N., Takahashi, F., Anderson, J.C., Ishihama, Y., Peck, S.C., and Shinozaki, K. (2013). Genetics and phosphoproteomics reveal a protein phosphorylation network in the abscisic acid signaling pathway in *Arabidopsis thaliana*. Sci. Signal. **6**:rs8.

Valli, A.A., Gallo, A., Rodamilans, B., López-Moya, J.J., and García, J.A. (2018). The HCPro from the *Potyviridae* family: an enviable multitasking Helper Component that every virus would like to have. Mol. Plant Pathol. **19**:744–763.

Verchot, J., and Carrington, J.C. (1995). Debilitation of plant potyvirus infectivity by P1 proteinase-inactivating mutations and restoration by second-site modifications. J. Virol. **69**:1582–1590.

Vogler, H., Kwon, M.-O., Dang, V., Sambade, A., Fasler, M., Ashby, J., and Heinlein, M. (2008). *Tobacco mosaic virus* movement protein enhances the spread of RNA silencing. PLoS Pathog. **4**:e1000038.

Wang, P., Xue, L., Batelli, G., Lee, S., Hou, Y.-J., Van Oosten, M.J., Zhang, H., Tao, W.A., and Zhu, J.-K. (2013). Quantitative phosphoproteomics identifies SnRK2 protein kinase substrates and reveals the effectors of abscisic acid action. Proc. Natl. Acad. Sci. U S A **110**:11205–11210.

Wang, S., Han, K., Peng, J., Zhao, J., Jiang, L., Lu, Y., Zheng, H., Lin, L., Chen, J., and Yan, F. (2019). *NbALD1* mediates resistance to turnip mosaic virus by regulating the accumulation of salicylic acid and the ethylene pathway in *Nicotiana benthamiana*. Mol. Plant Pathol. **20**:990–1004.

Wang, P., Hsu, C.-C., Du, Y., Zhu, P., Zhao, C., Fu, X., Zhang, C., Paez, J.S., Macho, A.P., Tao, W.A., et al. (2020). Mapping proteome-wide targets of protein kinases in plant stress responses. Proc. Natl. Acad. Sci. U S A **117**:3270–3280.

Wawer, I., Golisz, A., Sulkowska, A., Kawa, D., Kulik, A., and Kufel, J. (2018). mRNA decapping and 5'-3' decay contribute to the regulation of ABA signaling in *Arabidopsis thaliana*. Front. Plant Sci. **9**:312.

Westwood, J.H., McCann, L., Naish, M., Dixon, H., Murphy, A.M., Stancombe, M.A., Bennett, M.H., Powell, G., Webb, A.A.R., and Carr, J.P. (2013). A viral RNA silencing suppressor interferes with abscisic acid-mediated signalling and induces drought tolerance in *Arabidopsis thaliana*. Mol. Plant Pathol. **14**:158–170.

Xu, J., and Chua, N.-H. (2012). Dehydration stress activates *Arabidopsis* MPK6 to signal DCP1 phosphorylation. EMBO J. **31**:1975–1984.

Xu, M., Mazur, M.J., Tao, X., and Kormelink, R. (2020). Cellular RNA hubs: friends and foes of plant viruses. Mol. Plant Microbe Interact. **33**:40–54.

Yang, Z., and Li, Y. (2018). Dissection of RNAi-based antiviral immunity in plants. Curr. Opin. Virol. **32**:88–99.

Yang, Z., Huang, Y., Yang, J., Yao, S., Zhao, K., Wang, D., Qin, Q., Bian, Z., Li, Y., Lan, Y., et al. (2020). Jasmonate signaling enhances RNA silencing and antiviral defense in rice. Cell Host Microbe **28**:89–103.e8.

Yao, C., and Finlayson, S.A. (2015). Abscisic acid is a general negative regulator of *Arabidopsis* axillary bud growth. Plant Physiol. **169**:611–626.

Ying, X.-B., Dong, L., Zhu, H., Duan, C.-G., Du, Q.-S., Lv, D.-Q., Fang, Y.-Y., Garcia, J.A., Fang, R.-X., and Guo, H.-S. (2010). RNA-dependent RNA polymerase 1 from *Nicotiana tabacum* suppresses RNA silencing and enhances viral infection in *Nicotiana benthamiana*. Plant Cell **22**:1358–1372.

Yost, S.A., and Marcotrigiano, J. (2013). Viral precursor polyproteins: keys of regulation from replication to maturation. Curr. Opin. Virol. **3**:137–142.

Yu, X., Li, B., Jang, G.-J., Jiang, S., Jiang, D., Jang, J.-C., Wu, S.-H., Shan, L., and He, P. (2019). Orchestration of processing body dynamics and mRNA decay in *Arabidopsis* immunity. Cell Rep. **28**:2194–2205.e6.

Yusa, A., Neriya, Y., Hashimoto, M., Yoshida, T., Fujimoto, Y., Hosoe, N., Keima, T., Tokumaru, K., Maejima, K., Netsu, O., et al. (2019). Functional conservation of EXA1 among diverse plant species for the infection by a family of plant viruses. Sci. Rep. **9**:5958.

Zhang, J.-F., Yuan, L.-J., Shao, Y., Du, W., Yan, D.-W., and Lu, Y.-T. (2008). The disturbance of small RNA pathways enhanced abscisic acid response and multiple stress responses in *Arabidopsis*. Plant Cell Environ. **31**:562–574.

Zhang, X.-P., Liu, D.-S., Yan, T., Fang, X.-D., Dong, K., Xu, J., Wang, Y., Yu, J.-L., and Wang, X.-B. (2017). Cucumber mosaic virus coat protein modulates the accumulation of 2b protein and antiviral silencing that causes symptom recovery *in planta*. PLoS Pathog. **13**:e1006522.

Zhang, X., Dong, K., Xu, K., Zhang, K., Jin, X., Yang, M., Zhang, Y., Wang, X., Han, C., Yu, J., et al. (2018). *Barley stripe mosaic virus* infection requires PKA-mediated phosphorylation of γb for suppression of both RNA silencing and the host cell death response. New Phytol. **218**:1570–1585.

Zhang, T., Liu, P., Zhong, K., Zhang, F., Xu, M., He, L., Jin, P., Chen, J., and Yang, J. (2019). Wheat yellow mosaic virus NIb interacting with host light induced protein (LIP) facilitates its infection through perturbing the abscisic acid pathway in wheat. Biology **8**:E80.

Plant Communications, Volume *1*

Supplemental Information

Abscisic Acid Connects Phytohormone Signaling with RNA Metabolic Pathways and Promotes an Antiviral Response that Is Evaded by a Self-Controlled RNA Virus

Fabio Pasin, Hongying Shan, Beatriz García, Maren Müller, David San León, Márta Ludman, David H. Fresno, Károly Fátyol, Sergi Munné-Bosch, Guillermo Rodrigo, and Juan Antonio García

SUPPLEMENTAL METHODS

Transcriptomic analysis of *Nicotiana benthamiana* samples

Raw RNA-seq reads were filtered with Trimmomatic (Bolger et al., 2014) to remove poor quality reads and adapter contaminations. The remaining reads were mapped to the *Nicotiana benthamiana* transcriptome (Transcriptome assembly v5, primary transcripts (Nakasugi et al., 2014)) using Bowtie2 (Langmead and Salzberg, 2012) with the very-sensitive option activated. Transcript read counts were obtained by RSEM software (Li and Dewey, 2011), and rRNA counts were discarded. Differential expression analysis was calculated with edgeR and false discovery rates (FDR; Dataset_S1A) were computed by the Benjamini–Hochberg method (Robinson et al., 2010). Viral reads were mapped to a full-length PPV genome using HISAT2 (Kim et al., 2015); single nucleotide coverage was obtained using the igvtools `count` command (Thorvaldsdóttir et al., 2013). Cluster analyses were done using ClustVis (Metsalu and Vilo, 2015); when indicated, approximately unbiased and bootstrap *p* values were calculated by bootstrap resampling (1000 or 10000 replications) using Pvclust (Suzuki and Shimodaira, 2006). Gene list overlaps were visualized using euler*APE* (Micallef and Rodgers, 2014) and intersection plots were generated using UpSetR (Conway et al., 2017). Significance of gene list overlaps was determined by the hypergeometric test (upper cumulative distribution).

Gene functional annotations

To identify *Arabidopsis thaliana* homologs, *N. benthamiana* transcripts were used to search an *A. thaliana* protein database (TAIR10_pep_20101214_updated) with BLASTX (*e* value < 0.1); *N. benthamiana PR* transcripts were annotated on the basis of known *PR* genes (Dataset_S1B). Gene ontology (GO) classes associate to TAIR loci (version November 18, 2018) were obtained from the GO Consortium database [(The Gene Ontology Consortium, 2017); http://www.geneontology.org/gene-associations/]. TAIR loci associated to the GO:0003700 term were identified as transcription factors. GO classes containing "gene silencing" or "sirna" were searched in AmiGO [http://amigo.geneontology.org/amigo/search/ontology], and were used to identify gene silencing loci. GO classes containing the term "salicylic" were used to identify loci associated to salicylic acid; classes were filtered to remove those containing the terms "not depend upon salicylic acid signaling". The AgriGO webserver (Tian et al., 2017) was used to determine GO classes overrepresented within gene lists. Enrichment significance of GO terms was determined by Fisher's exact test and Hochberg correction.

Quantification of alternative splice events in *Arabidopsis thaliana* samples

Raw RNA-seq reads from time series ABA experiments (Song et al., 2016) were retrieved (SRP073711), and filtered with Trimmomatic (Bolger et al., 2014) to remove poor quality reads and adapter contaminations. The AtRTD2-QUASI (version AtRTDv2_QUASI_19April2016.fa), a high-quality *A. thaliana* transcriptome, was used as a reference (Zhang et al., 2017). Salmon 1.2.1 (Patro et al., 2017) was used for indexing using the `-keepDuplicates -k 31` options, and a *A. thaliana* Col-0 genome sequence obtained from ENSEMBL as a decoy. Isoform read counts were obtained by Salmon in the mapping-based mode, including the `--validateMappings --seqBias` options. Splice event coordinates were retrieved from AtRTDv2_QUASI_19April2016.gtf (Zhang et al., 2017) using SUPPA 2.1 (Trincado et al., 2018). The SUPPA `psiPerEvent` and `diffSplice` (including the `-m empirical -gc` options, and the `-th 1` filter as described (Love et al., 2018)) were used to identify differential alternative splicing events and event types; an adjusted $p < 0.05$ was used as a significance threshold (Dataset_S1D).

Generation of an augmented transcriptome assembly of *N. benthamiana* and its use in differential expression and splice analysis of RNA-seq samples

A reference genome dataset including host and viral sequences was obtained from the draft assembly Niben.genome.v1.0.1.contigs.fasta.gz of *N. benthamiana* genome (Bombarely et al., 2012), the pSN-PPV vector and the *nahG* gene (GenBank: M60055) sequences. *N. benthamiana* transcripts from Nbv5.1_transcriptome_primary_alternate_correct.fa.gz and NbDE transcriptome datasets (Nakasugi et al., 2014; Kourelis et al., 2019) were mapped to the reference genome dataset using Minimap2 in the splice mode (Li, 2018); gtf files were retrieved using StringTie with the `-R` option (Pertea et al., 2015). Transcripts from P1Pro- and PPV-infected *N. benthamiana* plants were obtained as described (Pertea et al., 2016). Briefly, raw RNA-seq reads were filtered with Trimmomatic (Bolger et al., 2014), mapped using the spliced aligner HISAT2 with the --dta option (Kim et al., 2015) against the reference genome dataset. Gtf files were retrieved using StringTie, which was used in the merge mode to obtain a final gtf file including transcript annotations from reference transcriptomes and those assembled from P1Pro- and PPV-infected samples. A padded version of transcript sequences was obtained using GffRead with `--w-add 200 -w` options (Zhang et al., 2017; Pertea and Pertea, 2020); this augmented transcriptome assembly of *N. benthamiana* was used in differential expression and splice analysis in P1Pro- and PPV-infected samples (Datasets S1F to S1H). Transcripts were quantified by Salmon (Patro et al., 2017); gene-level differential expression analysis was

performed using tximport and EdgeR (Robinson et al., 2010; Soneson et al., 2015); Cook's distance filtering was used to remove genes with outliers. Differential alternative splicing events and event types were identified by SUPPA 2.1 as described above (Dataset_S1H).

Mathematical model

A mathematical model based on four ordinary differential equations (ODE) was developed to describe the dynamics of plum pox virus in plants. The amounts of potyviral RNA (denoted by *R*), potyviral polyprotein (*Q*), potyviral processed protein (*P*), and host protein of the immune system (*S*) were considered as variables. The host plant (or a part of it, a leaf) was assumed as a single, uniform compartment in which the virus can replicate. Sigmoidal expressions were used to model the different biochemical processes underlying such replication following a generalized enzyme kinetics scheme in which both substrates and enzymes are limited in the medium (Rodrigo et al., 2011a). Parameter values are provided in Table S3.

In first place, the ODE for *R* reads

$$\frac{dR}{dt} = k_{syn}\frac{PR}{(\theta + P + R)(1+S)}\left(1 - \frac{R}{K}\right) - k_{sil}\frac{R^2}{\psi + \alpha P + R},$$

where two different terms were considered to construct it. The first term accounts for the synthesis of more potyviral RNA using the available molecules as a template through the action of viral replication proteins. This synthesis depends on both potyviral RNA and potyviral processed protein; k_{syn} is the viral RNA synthesis rate (in this case) and was assumed to be $k_{syn} = 3$ h^{-1} (i.e., three new viral genomes per hour), taking the same order of magnitude as in the case of an RNA virus infecting animals (Dahari et al., 2007). θ represents the protein-RNA dissociation constant, taking here $\theta = 20$ mol. That is, about 20 molecules of viral replication proteins are required to start the virus replication. The rate is nonetheless limited, on the one hand by the availability of resources, which we modeled in a logistic way. K denotes the maximal host resources available and its value was set to $K = 10^7$ mol, following a previous estimate (Martínez et al., 2011). On the other hand, viral RNA replication was assumed to be limited by action of the immune system (modeled by *S*). To simulate viral fitness after alteration of the RNA synthesis rate, the value of k_{syn} was adjusted by the correction factor τ, i.e. in the ODE for *R* we replaced k_{syn} by τk_{syn}.

The second term accounts for potyviral RNA degradation by the action of the RNA silencing machinery. The k_{sil} is the RNA silencing rate, here assumed to be $k_{sil} = 3$ h^{-1}, following the quantification in *Drosophila* (Haley and Zamore, 2004). This degradation depends on the amount of viral RNA, as well as potyviral processed protein (mostly HCPro, the viral suppressor of silencing). In our model, ψ represents the RNA silencing threshold; i.e., the amount of potyviral RNA from which the RNA silencing machinery starts. We empirically established $\psi = 10^4$ mol. When the amount of potyviral RNA is high enough ($R >> \psi$), this rate can be considered at first order ($k_{sil}R$). The presence of the viral suppressor of silencing increases this threshold, as this protein is able to block that machinery. We modeled this by correcting the value of ψ by αP, where α denotes the strength of suppression ($\alpha = 0.1$ for a strong suppressor and $\alpha < 0.1$ for a weak suppressor).

In second place, the ODE for *Q* reads

$$\frac{dQ}{dt} = k_{syn}R - \delta Q \,,$$

where only two simple terms (of first order) were considered. The first accounts for the production, and the second for the degradation. In this case, k_{syn} is the protein synthesis rate (i.e., three new potyviral polyproteins per hour). Note then that we assumed equal transcription and translation rates for simplicity. Moreover, δ is the protein degradation rate. In *A. thaliana*, rapidly-degrading proteins (as viral proteins are assumed to be) have half-lives of about one day (Li et al., 2017), so we took $\delta = 0.02$ h^{-1}.

In third place, the ODE for *P* reads

$$\frac{dP}{dt} = k_{clv}\frac{H}{1+H}\left(f_{clv}Q - P\right) - \delta P \,,$$

where the first part of the right-hand side accounts for the cleavage process of the potyviral polyprotein, which is host-dependent. k_{clv} is the potyviral polyprotein cleavage rate, here assumed to be $k_{clv} = 60$ h^{-1} (i.e., a very rapid process that takes on average just 1 min), in agreement with previous characterizations (Carrington et al., 1989). The process is not completed in totality, however, meaning that a small but significant fraction of polyproteins remains unaffected even at long times. We modeled this fact by introducing f_{clv}, the fraction of

cleaved protein at the equilibrium ($f_{clv} = 0.7$). The cleavage rate is therefore maximal at initial times and then decreases progressively (as long as *P* increases). In addition, *H* denotes the amount of a yet-unknown host factor essential for cleavage. This factor then limits the speed of the polyprotein processing. Here, we took $H = 0.001$ to model the wild-type virus scenario. The last part of the right-hand side, as before, corresponds to protein degradation. Note then that, for simplicity, we assumed equal polyprotein and protein degradation rates.

In fourth place, the ODE for *S* (which represents a protein amount normalized to the corresponding protein-DNA dissociation constant; perhaps a value close to θ) reads

$$\frac{dS}{dt} = k_{im}\left(\frac{P^n}{(\chi e^{\delta t})^n + P^n} + \frac{S^n}{1 + S^n}\right) - \delta S\,,$$

where one term composed of two subterms corresponds to the synthesis rate of the immune system protein and the last term corresponds to the degradation of that protein. For simplicity, we took the same degradation rate as before (δ). Production of the immune system protein is dependent on the presence of the potyviral processed protein in an amount sufficient to be sensed by the plant cell (modeled by the first subterm). In our model, χ represents the transcriptional threshold of the immune system; i.e., the amount of potyviral processed protein (*e.g.*, HCPro, CI, NIb, CP, etc.) from which the immune system machinery starts; empirically, we set $\chi = 10^8$ mol. The longer the time, however, the harder it is for the plant to mount this response, as the virus has more time to inhibit and/or subvert the host elements. Because of this extreme, we corrected the value of χ by a temporal exponential factor. In addition, the defense response was assumed to be maintained active once it has been mounted, through the action of positive feedback (modeled by the second subterm). k_{im} is the maximal synthesis rate of *S*. We considered $k_{im} = 0.2$ h^{-1}, leading to protein amounts similar to those previously considered to model a gene regulatory network in plants (Rodrigo et al., 2011b). Finally, *n* denotes the Hill coefficient of this regulation (here, $n = 4$).

Numerical simulations to obtain viral infection dynamics were carried out with MATLAB (MathWorks). Different scenarios (corresponding to different virus clones) were modeled by changing key parameter values. For example, to model an HCPro mutant, we replaced $\alpha = 0.1$ with $\alpha = 0$ (i.e., no suppression); to model a clone lacking the P1 autoinhibitory domain (P1Pro) and its uncontrolled self-cleavage, we replaced $H = 0.001$ with $H \to \infty$ (i.e., host-independent cleavage).

SUPPLEMENTAL FIGURES

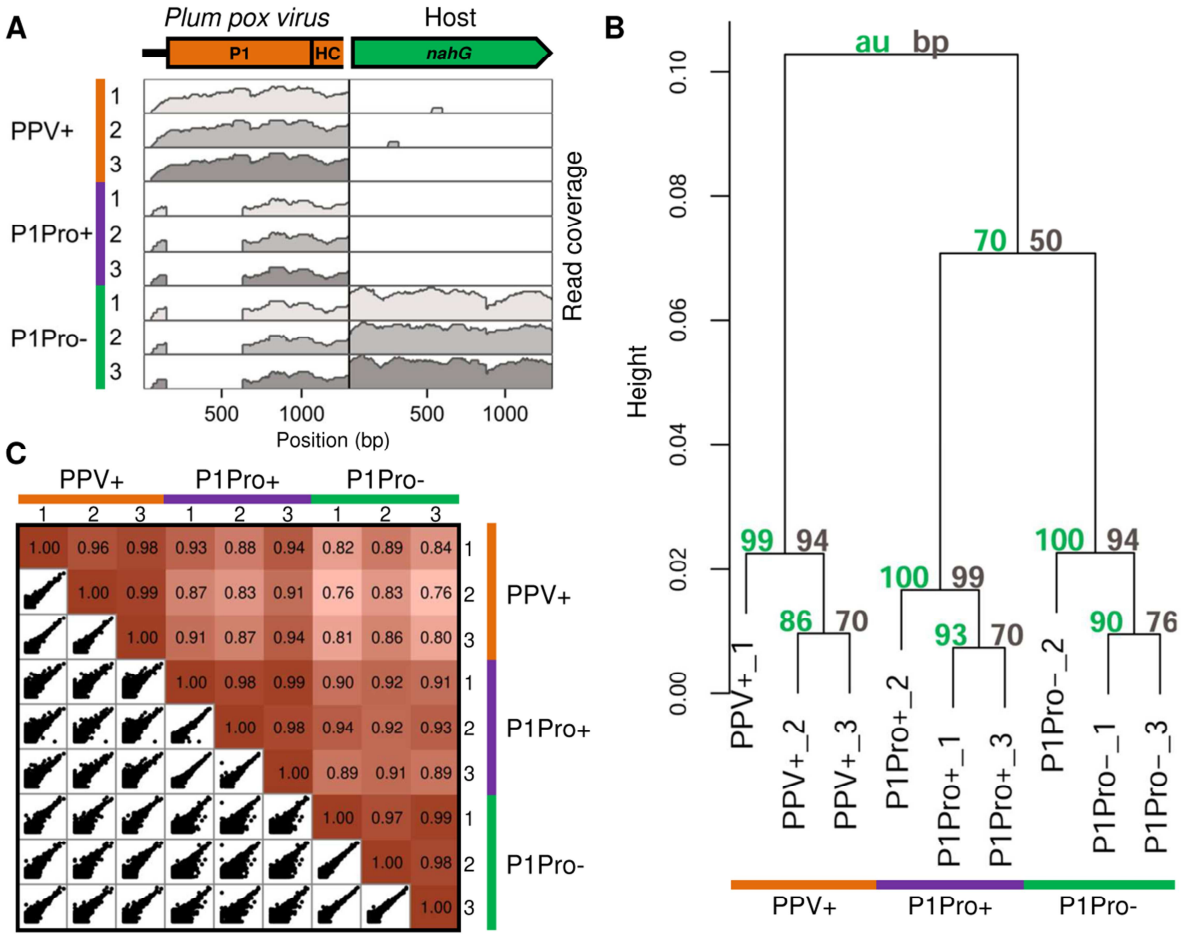

Supplemental Figure 1. Quality control of RNA-seq samples.

(A) Read coverage (log10 scale) of the 5' terminus of the PPV genome and coding sequence of the *nahG* transgene (GenBank: M60055).

(B) Confidence of the unsupervised multivariate analysis and sample grouping shown in Figure 1C. Clustering dendrogram and probability values are indicated (au, approximately unbiased; bp, bootstrap probability).

(C) Correlation values and plots of the biological replicates analyzed by RNA-seq. Counts of differentially regulated transcripts (FDR < 0.05 in two-way comparisons) in at least one comparison were used to compute Pearson's *r* values.

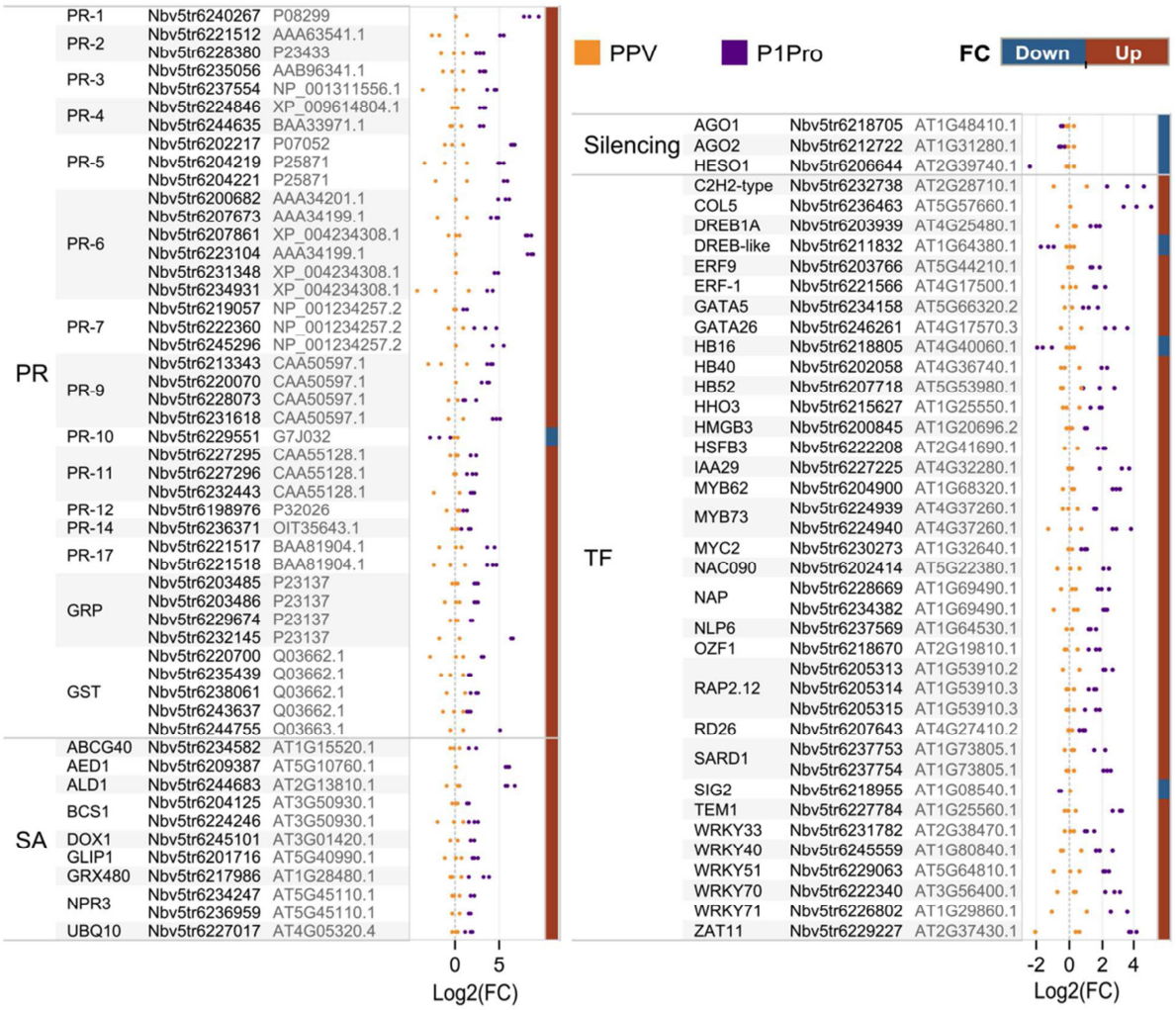

Supplemental Figure 2. Defense marker and transcription factor genes differentially regulated by P1Pro with respect to PPV.

Functional annotation of differentially expressed transcripts of wild-type *N. benthamiana* plants infected with PPV or P1Pro was carried out by searching known pathogenesis-related protein (PR) and *Arabidopsis thaliana* sequences; SA, salicylic acid-related genes; Silencing, RNA silencing genes; TF, transcription factors. For each transcript, the symbol, the accession codes of the *N. benthamiana* gene, and reference homologs are indicated; expression values using PPV mean value as reference are plotted for each biological replicate ($n = 3$), and colored according to the experimental condition analyzed (PPV, orange; P1Pro, purple); red or blue boxes highlight up- or downregulated transcripts, respectively; only transcripts with an FDR < 0.01 are shown.

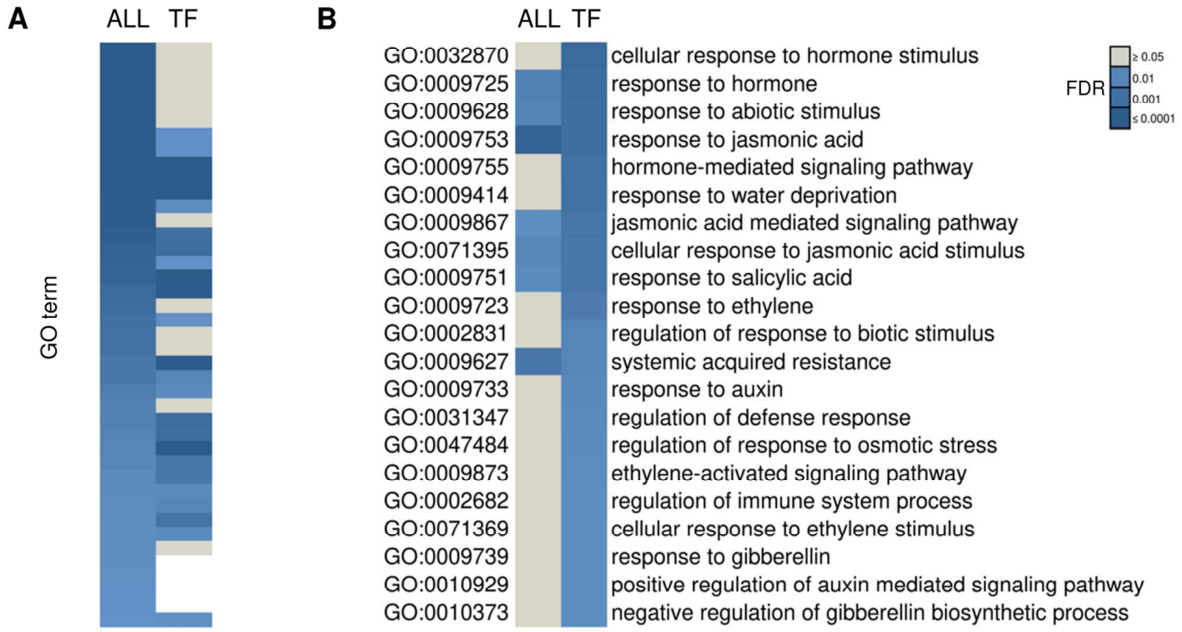

Supplemental Figure 3. Enrichment of functional categories in genes differentially regulated by P1Pro with respect to PPV.

Differentially expressed transcripts (FDR < 0.05) of wild-type *N. benthamiana* plants infected with PPV or P1Pro (P1Pro+/PPV+ comparison) were analyzed.

(A) Significance value of gene ontology (GO) terms enriched in the differentially expressed transcripts (ALL transcripts); the GO significance value is also shown for the subset including only genes encoding transcription factors (TF).

(B) GO terms enriched in the TF subset along with their significance value by ALL transcript analysis. Color scale shows enrichment significance by Fisher's exact test with Hochberg's FDR correction.

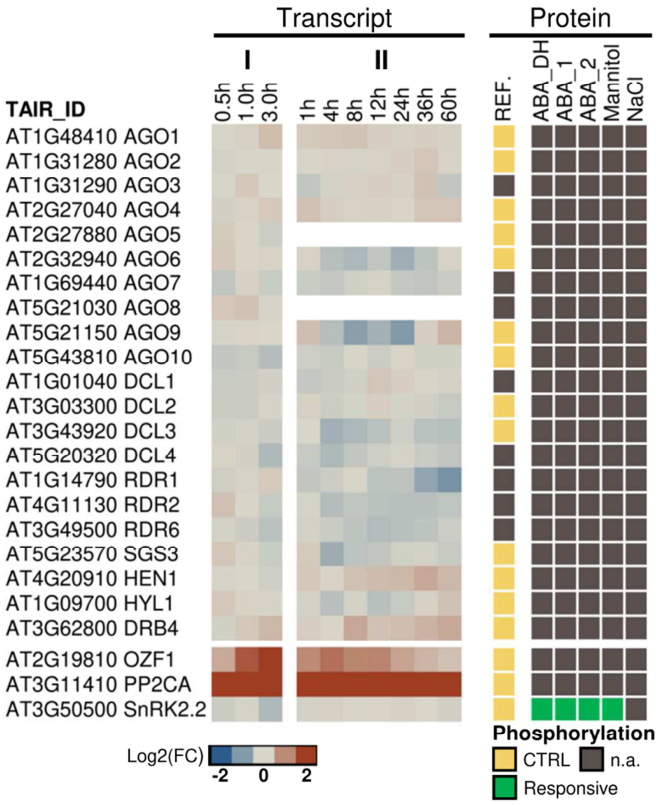

Supplemental Figure 4. Transcriptional and post-translational effects of ABA on the antiviral RNA silencing.

Right, *A. thaliana* accession numbers of the major antiviral RNA silencing components. Center, time-course analysis of transcript fold-changes in *A. thaliana* seedlings treated with ABA; I, microarray study (Nemhauser et al., 2006); II, RNA-seq study (Song et al., 2016). Right, phosphorylation responsiveness of RNA silencing protein after ABA and dehydration (ABA_DH), ABA (ABA_1, ABA_2), mannitol or NaCl treatments (Umezawa et al., 2013; Wang et al., 2013; Wang et al., 2020); a comprehensive phosphoproteome dataset (REF.) was used as a control of known phophoproteins (Mergner et al., 2020). *OZF1* and *PP2CA* are included as ABA-inducible transcript controls; SnRK2.2 as a protein of which phosphorylation status is ABA responsive.

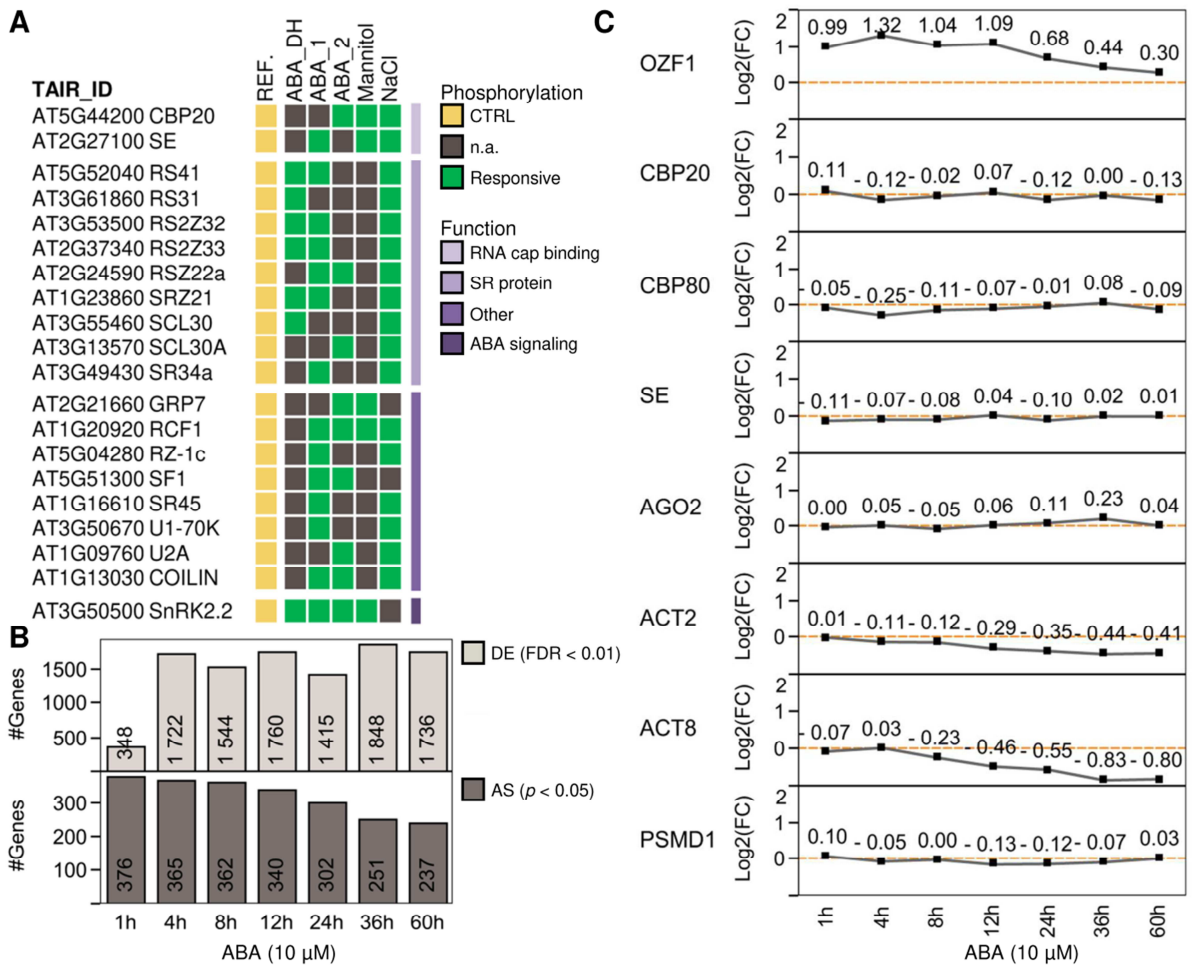

Supplemental Figure 5. ABA-dependent regulation of host mRNA splicing.

(A) Phosphorylation responsiveness of *A. thaliana* proteins implicated in constitutive and alternative splicing after ABA and dehydration (ABA_DH), ABA (ABA_1, ABA_2), mannitol or NaCl treatments (Umezawa et al., 2013; Wang et al., 2013; Wang et al., 2020); a comprehensive phosphoproteome dataset (REF.) was used as a control of known phophoproteins (Mergner et al., 2020). Serine/arginine-rich (SR) splicing factors were annotated according to Barta et al. (2010); SnRK2.2, protein of which phosphorylation status is ABA responsive.

(B) Time-course analysis of genes differentially expressed (DE, FDR < 0.01), and genes with alternative splicing events significantly altered (AS, $p < 0.05$) in *A. thaliana* seedlings treated with ABA.

(C) Time-course, ABA-dependent transcriptional regulation of selected genes in *A. thaliana*. Fold-changes are shown of an ABA-inducible transcript (OZF1, AT2G19810), components

(CBP20, AT5G44200; CBP80, AT2G13540) or interactors (SE, AT2G27100) of the nuclear cap-binding complex, an RNA silencing gene (AGO2, AT1G31280), reference genes commonly used in RT-qPCR assays (ACT2, AT3G18780; ACT8, AT1G49240), and a gene whose abundance show small fluctuations under ABA treatment (PSMD1, AT2G32730). Time series RNA-seq data were used (Song et al., 2016).

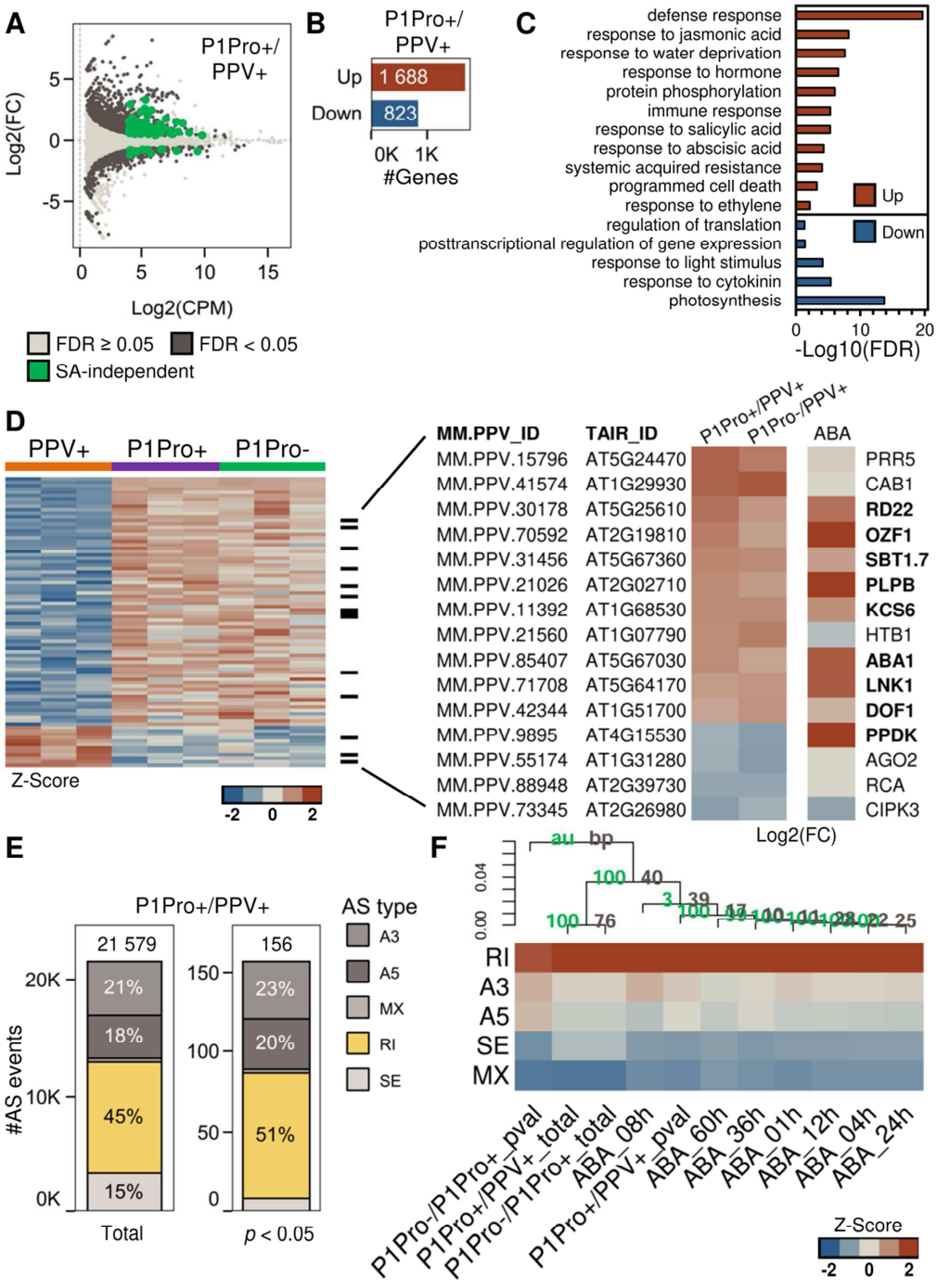

Supplemental Figure 6. An augmented transcriptome assembly of *N. benthamiana* enhanced the analysis of P1Pro-induced responses.

RNA-seq reads from P1Pro and PPV-infected *N. benthamiana* plants were used for *de novo* assembly of host transcripts. The transcriptome obtained was merged with reported datasets, and used in gene expression and splice event analysis of wild-type *N. benthamiana* plants agro-

inoculated with PPV (PPV+) or P1Pro clones (P1Pro+), and *nahG*-expressing plants with P1Pro (P1Pro-).

(A) Gene-level fold-changes and coverage values of the P1Pro+/PPV+ transcriptomic comparison. Differentially expressed genes are marked (FDR < 0.05); the green dots indicate a subset of genes that are altered in P1Pro-infected wild-type plants, but not in *nahG*-transgenic plants (where SA signaling is down-regulated; i.e., SA-independent genes).

(B) Number of differentially expressed genes identified in the P1Pro+/PPV+ comparison.

(C) Selected GO terms enriched in genes up- or down-regulated in the P1Pro+/PPV+ comparison.

(D) Left, normalized read counts (heatmap; $n = 3$) of the SA-independent gene subset. Right, representative genes from the SA-independent subset and their fold-changes in the P1Pro+/PPV+ or P1Pro-/PPV+ comparisons are shown along with expression values of their *A. thaliana* homologs after ABA treatment (Nemhauser et al., 2006).

(E) Alternative splice (AS) events identified in the P1Pro+/PPV+ comparison. Ratios of AS types are plotted: SE, skipping exon; RI, retained intron; MX, mutually exclusive exon; A5, alternative 5' splice site; A3, alternative 3' splice site. AS event numbers and type ratios are shown for all the events identified (Total) or only those significantly altered (adjusted $p < 0.05$).

(F) Hierarchical clustering of normalized ratios of the AS types identified by analysis of our samples, or RNAseq data from ABA-treated *A. thaliana* plants; cluster probabilities are indicated (au, approximately unbiased; bp, bootstrap probability).

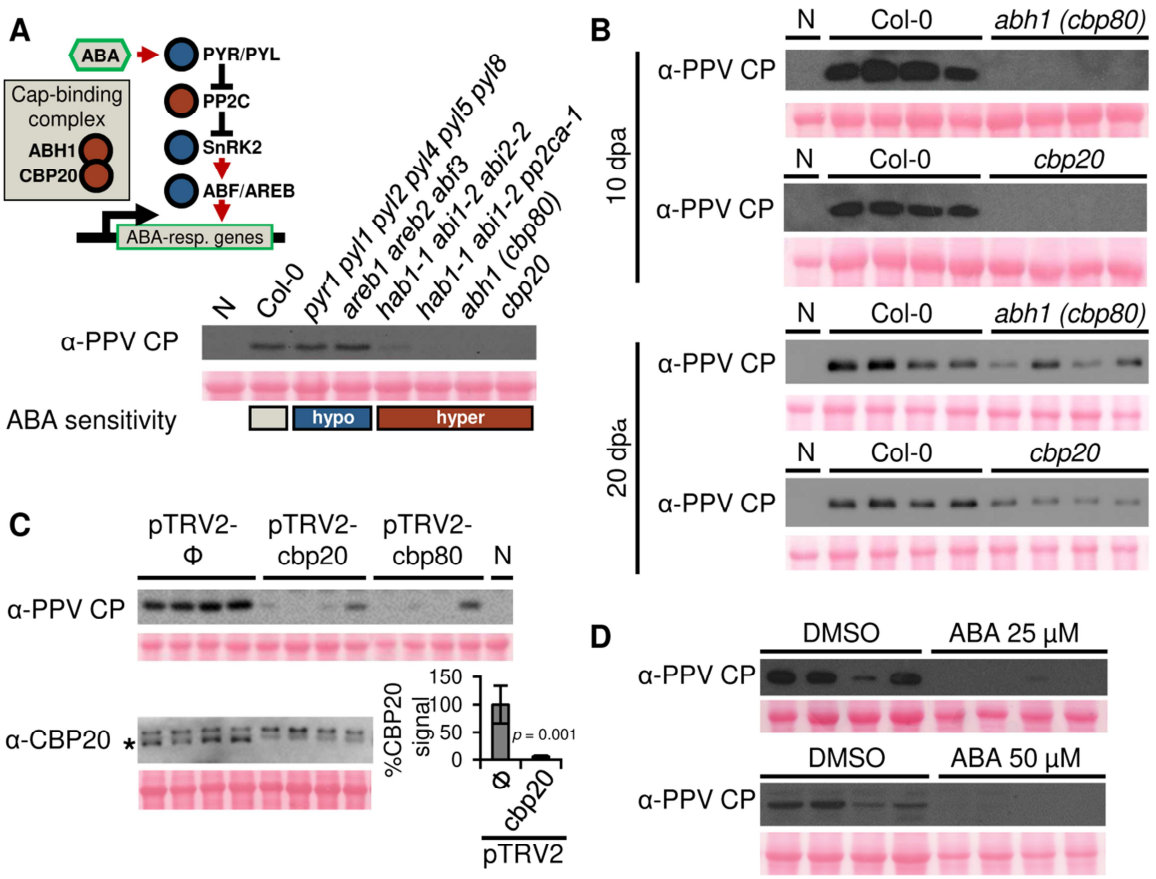

Supplemental Figure 7. ABA and RNA metabolic defects promote resistance to plum pox virus (PPV).

(A) Top, diagram of ABA signaling components; arrows and T-bars indicate positive and negative interactions, respectively. Bottom, immunoblot shows PPV coat protein (CP) accumulation in *A. thaliana* mutant lines at 14 days post agro-inoculation (dpa); the Col-0 accession and its mutant lines *pyr1 pyl1 pyl2 pyl4 pyl5 pyl8* (Gonzalez-Guzman et al., 2012), *areb1 areb2 abf3* (Yoshida et al., 2010), *hab1-1 abi1-2 abi2-2* and *hab1-1 abi1-2 pp2ca-1* (Rubio et al., 2009), *abh1(cbp80)* (Hugouvieux et al., 2001), and *cbp20* (Papp et al., 2004) were used. ABA perception of the lines screened is indicated: hypo- (blue) and hypersensitive (red); N, non-treated sample.

(B) PPV accumulation in *A. thaliana abh1(cbp80)* and *cbp20* lines at 10 and 20 dpa. Anti-PPV CP immunoblots are shown; for quantification values, see Figure 5A.

(C) VIGS of cap-binding complex genes in *N. benthamiana*. The pTRV2-cbp20 or pTRV2-cbp80 vectors were delivered to target *NbCBP20* and *NbCBP80* transcripts, respectively; pTRV2-Φ, empty vector control. TRV-treated plants were inoculated with PPV. The anti-PPV CP

immunoblot is shown; for quantification values, see Figure 5D. Bottom, immunoblot using anti-CBP20 serum. The asterisk marks a major band that is absent in pTRV2-cbp20 samples; band quantification is plotted (mean ± SD, $n = 4$); p value is indicated (Student's t test); N, non-treated sample.

(D) PPV accumulation after ABA treatments. Anti-PPV CP immunoblot of samples from plants treated with 25 μM ABA or DMSO solutions; for quantification values, see Figure 5E. Anti-PPV CP immunoblot of samples from plants treated with 50 μM ABA or DMSO solutions. Ponceau red-stained blots are shown as loading controls.

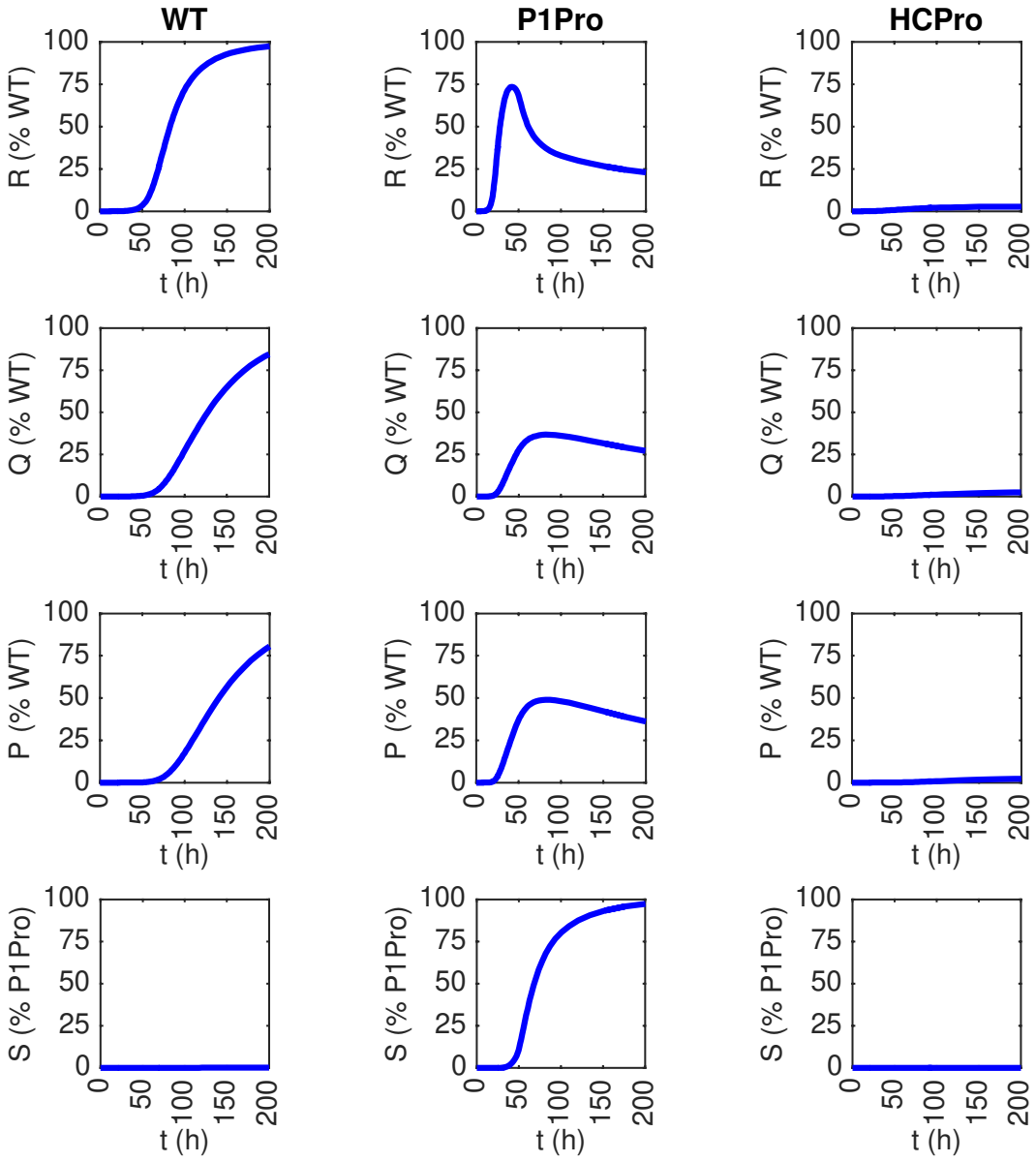

Supplemental Figure 8. Simulations of infection dynamics.

Virus RNA (*R*), potyviral polyprotein (*Q*), potyviral processed protein (*P*), and host protein of the immune system (S) are plotted for scenarios of three different clones: self-controlled, wild-type PPV (WT, left); a clone lacking the P1 autoinhibitory domain and with uncontrolled self-cleavage (P1Pro, center); and a mutant clone with an HCPro with no suppression activity (HCPro, right).

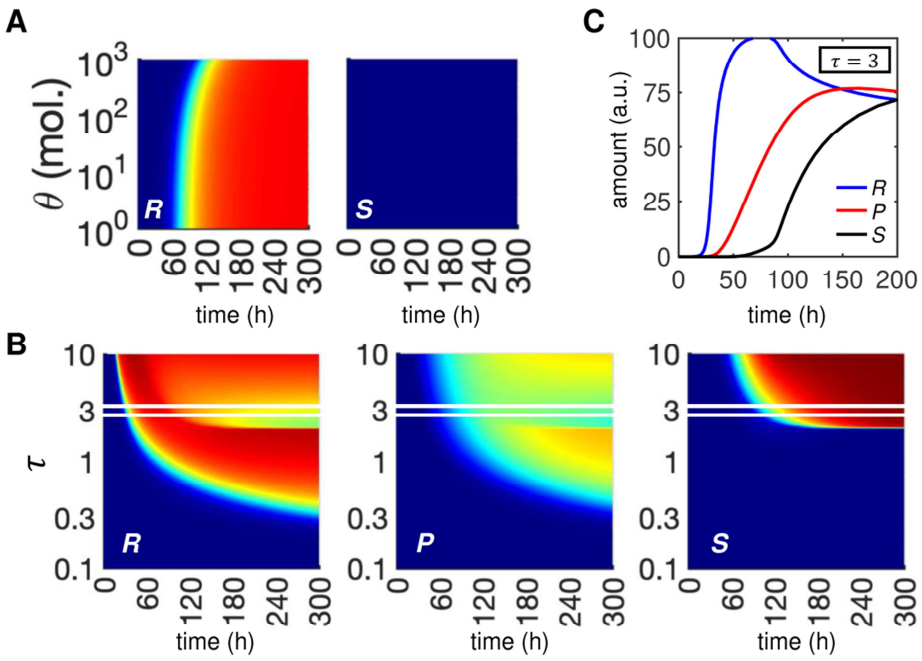

Supplemental Figure 9. Simulations of viral load and immune response dynamics for varying efficiency of viral replication.

Dynamics were modeled for varying RNA binding constant (θ) of the viral replicase or for the viral RNA synthesis rate (k_{syn}) adjusted by the correction factor τ (i.e. τk_{syn}). Numerical simulations of viral RNA (*R*), mature protein (*P*) and immune response (*S*) levels are shown for the wild-type PPV scenario, i.e. the virus clone with a self-controlled polyprotein processing.

(A) Time-course simulations of the *R*, and *S* accumulation relative to the maximum (dark blue for 0% and dark red for 100%) are shown for varying RNA binding constant (θ) of the replicase.

(B) Time-course simulations of the *R*, *P*, and *S* accumulation relative to the maximum (dark blue for 0% and dark red for 100%) are shown for varying RNA synthesis rate. The $\tau = 3$ value is marked and its dynamics are plotted in panel C. (**C**) The *R*, *P*, and *S* dynamics for $\tau = 3$.

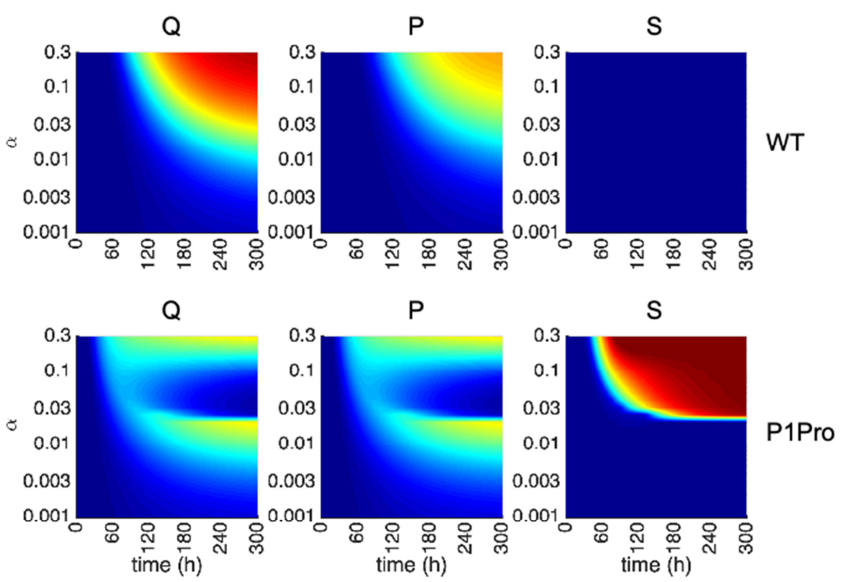

Supplemental Figure 10. Simulations of expression dynamics for varying strength of suppression.

Time-course simulations of viral polyprotein (*Q*) and mature protein (*P*), and immune response (*S*) levels are shown as % relative to the maximum; dark blue for 0% and dark red for 100%. The wild-type PPV (WT, top), and the uncontrolled self-cleavage (P1Pro, bottom) scenarios are shown; α, strength of the RNA silencing suppression.

SUPPLEMENTAL TABLES

Supplemental Table 1. Salicylic acid-independent genes differentially expressed in P1Pro+/PPV+ and P1Pro-/PPV+ comparisons

Transcript*			P1Pro+/PPV+		P1Pro-/PPV+	
SYDNEY_ID[#]	TAIR_ID	TAIR_Symbol	Log2(FC)	FDR	Log2(FC)	FDR
Nbv5tr6236463	AT5G57660	COL5	6.32	1.0E-03	6.10	5.3E-03
Nbv5tr6208832	n.a.	n.a.	4.19	5.9E-14	4.18	2.3E-13
Nbv5tr6199225	AT2G07777	n.a.	3.54	3.6E-40	3.56	8.2E-39
Nbv5tr6226581	n.a.	n.a.	2.09	1.3E-18	2.09	1.1E-12
Nbv5tr6241923	AT1G29930	CAB1	1.86	2.3E-14	2.16	2.3E-12
Nbv5tr6243964	n.a.	n.a.	1.77	6.5E-05	1.84	1.5E-04
Nbv5tr6236418	AT5G24470	PRR5	1.59	7.4E-08	1.31	3.3E-04
Nbv5tr6236294	AT1G29930	CAB1	1.58	1.7E-07	2.19	8.0E-10
Nbv5tr6206822	n.a.	n.a.	1.49	9.2E-03	1.51	1.4E-02
Nbv5tr6218670	AT2G19810	OZF1	1.40	1.6E-06	1.02	1.3E-02
Nbv5tr6207355	AT1G29930	CAB1	1.33	5.2E-09	1.83	5.1E-12
Nbv5tr6212008	AT5G66150	n.a.	1.28	3.0E-05	1.08	7.2E-03
Nbv5tr6215695	n.a.	n.a.	1.27	4.5E-15	0.93	8.0E-05
Nbv5tr6218584	AT1G06760	H1.1	1.25	3.4E-02	1.47	2.9E-02
Nbv5tr6236371	AT1G27950	LTPG1	1.24	6.8E-03	1.41	6.9E-03
Nbv5tr6216301	n.a.	n.a.	1.21	1.8E-03	1.29	7.3E-03
Nbv5tr6236193	AT5G25610	RD22	1.12	7.1E-07	0.67	2.4E-02
Nbv5tr6206135	AT1G29930	CAB1	1.12	2.1E-05	1.84	1.9E-11
Nbv5tr6198976	AT1G61070	LCR66	1.04	2.3E-03	1.32	6.7E-05
Nbv5tr6204947	AT2G02710	PLPB	1.02	8.3E-07	0.83	1.4E-03
Nbv5tr6229630	AT2G05070	LHCB2.2	1.00	1.2E-02	1.67	3.4E-08
Nbv5tr6219057	AT5G67360	SBT1.7	1.00	5.7E-05	1.04	1.9E-04
Nbv5tr6241941	AT2G34430	LHB1B1	0.95	5.4E-05	1.63	1.0E-12
Nbv5tr6233144	AT4G37800	XTH7	0.87	1.4E-03	1.25	3.6E-10
Nbv5tr6241860	AT1G29930	CAB1	0.83	2.2E-02	1.05	3.1E-02
Nbv5tr6226195	AT1G68530	KCS6	0.83	2.0E-02	0.87	2.4E-02
Nbv5tr6241423	AT1G07790	HTB1	0.76	4.3E-02	1.01	2.9E-03
Nbv5tr6245715	ATMG01190	ATP1	0.63	2.2E-09	0.37	7.9E-03
Nbv5tr6206813	ATMG00090	RPS3	0.47	1.0E-02	0.41	3.0E-03
Nbv5tr6212722	AT1G31280	AGO2	-0.66	7.6E-03	-0.88	5.0E-04
Nbv5tr6230075	AT4G15530	PPDK	-0.68	5.2E-03	-0.92	7.4E-03
Nbv5tr6236236	ATCG01250	NDHB.2	-1.03	3.4E-06	-0.76	9.4E-03
Nbv5tr6202574	AT5G17100	n.a.	-1.18	4.6E-06	-0.97	1.1E-03
Nbv5tr6230855	ATCG00490	RBCL	-1.21	1.9E-02	-1.35	3.9E-05
Nbv5tr6246056	ATCG00720	PETB	-1.21	3.0E-02	-1.57	6.3E-03
Nbv5tr6202627	AT1G30760	ATBBE-LIKE 13	-1.23	2.3E-05	-0.75	4.3E-02
Nbv5tr6200121	ATCG00680	PSBB	-1.39	4.7E-05	-1.02	3.4E-02
Nbv5tr6241933	AT1G47128	RD21A	-2.27	3.5E-02	-4.17	2.8E-03
Nbv5tr6221690	AT4G13010	CEQORH	-6.29	1.4E-02	-6.20	3.7E-02

*n.a., not applicable; no TAIR gene with BLASTX *e* value < 0.1, or no gene symbol available
[#]Accession numbers of *N. benthamiana* transcripts (Nakasugi et al., 2014)

Supplemental Table 2. AGO2 tryptic peptide quantification in PPV and P1Pro-infected plant samples

Protein		Peptide					Quantification*			
SYDNEY_ID	Symbol	Sequence	Modification	mz#	z#	m#	PPV 115	PPV 117	P1Pro 114	P1Pro 116
Nbv5tr6212722	AGO2	(R)DVQPNSSEASTVR(Q)	iTRAQ4plex	767.38	2	1532.75	0.00	0.02	-1.19	-0.60

*Biological replicates (n = 2) were labeled with the iTRAQ tag indicated (PPV, 115 and 117; P1Pro, 114 and 116). Quantification values are expressed in Log2(FC) using the 115-tagged PPV sample as a reference.
#Experimental

Supplemental Table 3. Summary of parameter values used for mathematical modeling

Parameter	Value	Parameter	Value
k_{syn}	3 h^{-1}	k_{sil}	3 h^{-1}
θ	20 mol.	ψ	10^4 mol.
K	10^7 mol.	α	0.1 0 (HCPro)
δ	0.02 h^{-1}	H	0.001 ∞ (P1Pro)
k_{clv}	60 h^{-1}	f_{clv}	0.7
k_{im}	0.2 h^{-1}	n	4
χ	10^8 mol.		

Supplemental Table 4. Plasmids used in the study

ID	Description	Reference
pSN-PPV	Infectious clone of a GFP-tagged plum pox virus (PPV) isolate adapted to *Nicotiana* spp., and suitable for *Agrobacterium*-mediated infection	(Pasin et al., 2014)
pSN-PPV P1Pro[V164]	pSN-PPV-based clone with the truncated P1 lacking residues 2-163 (herein, the P1Pro clone)	(Pasin et al., 2014)
pGr208	Potato virus X (PVX) infectious clone	(Peart et al., 2002)
pTRV1	TRV RNA1 vector (YL192)	(Liu et al., 2002)

pTRV2-Φ	TRV RNA2 silencing vector (also known as pTRV2-MCS or YL156; GenBank:AF406991)	(Liu et al., 2002)
pBTEX::avrPtoB	Binary vector for transient expression of the HopAB2 (AvrPtoB) effector from the *Pseudomonas syringae* pv. tomato DC3000 strain	(Kim et al., 2002)
pSN.5 P1|HC-Stop	Binary vector for transient expression of the full-length PPV P1 and HCPro cistrons, and flanked by PPV 5' and 3' UTRs	(Pasin et al., 2014)
pSN.5 P1Pro|HC-Stop	Binary vector for transient expression of a PPV P1 version lacking residues 2-163, the full-length HCPro cistron, and flanked by PPV 5' and 3' UTRs	(Pasin et al., 2014)
pSN.5 P1Pro-Stop	Binary vector for transient expression of a PPV P1 version lacking the 2-163 residues, no HCPro cistron, and flanked by PPV 5' and 3' UTRs	This study
pSN.5 AvrPtoB#3	Binary vector for transient expression of a version of the HopAB2 effector flanked by PPV 5' and 3' UTRs; subcloned from the pBTEX::avrPtoB	This study
pTRV2-cbp20	TRV RNA2 silencing vector including a cDNA fragment of the *N. benthamiana* Nbv5tr6270933 gene (*NbCBP20*). Plant total RNA was used in RT-PCR reactions; a 442-bp fragment of *NbCBP20* was amplified using X277_F/X278_R primers and inserted into the XmaI/XbaI-digested pTRV2-Φ vector by one-step isothermal assembly (Gibson et al., 2009) to yield pTRV2-cbp20.	This study
pTRV2-cbp80	TRV RNA2 silencing vector including a cDNA fragment of the *N. benthamiana* Nbv5tr6236567 gene (*NbCBP80*). Plant total RNA was used in RT-PCR reactions; a 426-bp fragment of *NbCBP80* was amplified using X275_F/X276_R primers, and inserted into the XmaI/XbaI-digested pTRV2-Φ vector by one-step isothermal assembly (Gibson et al., 2009) to yield pTRV2-cbp80.	This study

Supplemental Table 5. Sequences of the primers used

ID	Sequence*	Use
X275_F	ccgtagtttaatgtcttcgggacatgCATATTACACATTGGTTATCATCG	Cloning
X276_R	gattctgtgagtaaggttaccTaattctCCTTTCACCATGTCCTTCAGC	Cloning
X277_F	ccgtagtttaatgtcttcgggacatgCTGTCAAAcATATCAGCGGGAC	Cloning
X278_R	gattctgtgagtaaggttaccTaattCTCTCACGGAAACGTGGATT	Cloning
2174_F	CCTTAATTTCTCTACCAAATTTACTGC	RT-PCR
1631_R	GCACAAGAACTATAACCCGAATGG	RT-PCR
REF_1_F	GCTGCTCTAGGAACTGCTGATGA	RT-qPCR
REF_1_R	TACCTtGTGCCAAACCCCTGAT	RT-qPCR
CBP20_F	TCGTGCTGGAGAGATTAAAAAGATAGT	RT-qPCR
CBP20_R	CGAATAGGGCGATCATCAAGAA	RT-qPCR
CBP80_F_1095	AGAGTATTTGTTGGATGTGCTTTTATT	RT-qPCR
CBP80_R_1277	GCCCCTGcCAGAGCCTTG	RT-qPCR
OZF1_F	AGCCCATCAACATTCCGACC	RT-qPCR
OZF1_R	CCTTCCAGATTCTACCCTCTCCAT	RT-qPCR

*Mismatched nucleotides in lower case

Supplemental Table 6. Gene-specific primers used in qRT-PCR assays

SYDNEY_ID	TAIR_ID	Symbol	Forward	Reverse	Product size
Nbv5tr6218939	AT2G32730	NbPSMD1	REF_1_F	REF_1_R	202bp
Nbv5tr6270933	AT5G44200	NbCBP20	CBP20_F	CBP20_R	153bp
Nbv5tr6236567	AT2G13540	NbCBP80	CBP80_F_1095	CBP80_R_1277	207bp
Nbv5tr6218670	AT2G19810	NbOZF1	OZF1_F	OZF1_R	144bp

Supplemental Table 7. Sequences of the *N. benthamiana* cDNA fragments used in VIGS assays

Construct	Sequence*
pTRV2-cbp20	ctgtgagtaaggttacctaattCTCTCACGGAAACGTGGATTCTTCTCCGGTCTGGACTCGTGATCA GAGTTTCTTCGAGATTCACGGTCATAACTCCTCTTTGGATAATCTGACCGATGGCGGTCATCTTCCC TGTGTCGCTTGCGTTGATAGTCTCTACCGTGTCGATAAGAACCTCCATGACCTTGATTTCCACCATG TCTACCATAGTGAGGTGGCGGCATAACCGGTGGGTAACCGCCCAATGATCCTGTACCATAATCCACT AGCTGCCTTTGTGCTTCCAACTCCTTTTGGACCAATTTTCCATAACCACCTCGACCTGGATCGTAGT CAGTACGATATTCGTCGCGCACCTGTCCACCACTCCTACCACGGCCCCATTGCCTACCTTCTTGAAA TCCCCAGTCAAAATCCACACGAATAGGGCGATCATCAAGAATTGTCCCGCTGATATGTTTGACAGca tgtcccgaagacattaaactac
pTRV2-cbp80	ctgtgagtaaggttacctaattctCCTTTCACCATGTCCTTCAGCTCTACAGAGAGTGCACGCTCAG TTGGATCTGTACCATCTTCTGCACTATATTTAAACTGTGGTCCACCTCTCGGTGGAAGTAACTCCTC CAAAGCAGGGGTGTTCTCAATGCTCTGCTTGATTTTGTCCCAATATGAAAGACGGACTTCTCTTTCC AAAACCTCTTGAACAAACACACGCTGTGGGGCCCATTTTGGCAGATCTAACACATGAGCCCATTCTT CCCATGGCCAGATAAATTGAAAGTTTGACAAATGATGTGAGAACCAAAGGATGAGACGTGTTCGGCA TTCCATGTCTAAATCTGCTATTTTATCAAAAAGAGCACGGACAGCCCCAGCTACAACCGCTGGAAAG GCCCCTGGCAGAGCCTTGCATAAATCGATGATAACCAATGTGTAATATGcatgtcccgaagacatta aactac

*Upper case, *N. benthamiana* cDNA sequence cloned; lower case, pTRV2 vector sequence

SUPPLEMENTAL REFERENCES

Barta, A., Kalyna, M., and Reddy, A. S. N. (2010). Implementing a rational and consistent nomenclature for serine/arginine-rich protein splicing factors (SR proteins) in plants. *Plant Cell* 22:2926–2929.

Bolger, A. M., Lohse, M., and Usadel, B. (2014). Trimmomatic: a flexible trimmer for Illumina sequence data. *Bioinforma. Oxf. Engl.* 30:2114–2120.

Bombarely, A., Rosli, H. G., Vrebalov, J., Moffett, P., Mueller, L. A., and Martin, G. B. (2012). A draft genome sequence of *Nicotiana benthamiana* to enhance molecular plant-microbe biology research. *Mol. Plant. Microbe Interact.* 25:1523–1530.

Carrington, J. C., Freed, D. D., and Sanders, T. C. (1989). Autocatalytic processing of the potyvirus helper component proteinase in *Escherichia coli* and in vitro. *J. Virol.* 63:4459–4463.

Conway, J. R., Lex, A., and Gehlenborg, N. (2017). UpSetR: an R package for the visualization of intersecting sets and their properties. *Bioinforma. Oxf. Engl.* 33:2938–2940.

Dahari, H., Ribeiro, R. M., Rice, C. M., and Perelson, A. S. (2007). Mathematical modeling of subgenomic hepatitis C virus replication in Huh-7 cells. *J. Virol.* 81:750–760.

Gibson, D. G., Young, L., Chuang, R.-Y., Venter, J. C., Hutchison III, C. A., and Smith, H. O. (2009). Enzymatic assembly of DNA molecules up to several hundred kilobases. *Nat. Methods* 6:343–345.

Gonzalez-Guzman, M., Pizzio, G. A., Antoni, R., Vera-Sirera, F., Merilo, E., Bassel, G. W., Fernández, M. A., Holdsworth, M. J., Perez-Amador, M. A., Kollist, H., et al. (2012). *Arabidopsis* PYR/PYL/RCAR receptors play a major role in quantitative regulation of stomatal aperture and transcriptional response to abscisic acid. *Plant Cell* 24:2483–2496.

Haley, B., and Zamore, P. D. (2004). Kinetic analysis of the RNAi enzyme complex. *Nat. Struct. Mol. Biol.* 11:599–606.

Hugouvieux, V., Kwak, J. M., and Schroeder, J. I. (2001). An mRNA cap binding protein, ABH1, modulates early abscisic acid signal transduction in *Arabidopsis*. *Cell* 106:477–487.

Kim, Y. J., Lin, N. C., and Martin, G. B. (2002). Two distinct *Pseudomonas* effector proteins interact with the Pto kinase and activate plant immunity. *Cell* 109:589–598.

Kim, D., Langmead, B., and Salzberg, S. L. (2015). HISAT: a fast spliced aligner with low memory requirements. *Nat. Methods* 12:357–360.

Kourelis, J., Kaschani, F., Grosse-Holz, F. M., Homma, F., Kaiser, M., and van der Hoorn, R. A. L. (2019). A homology-guided, genome-based proteome for improved proteomics in the alloploid *Nicotiana benthamiana*. *BMC Genomics* 20:722.

Langmead, B., and Salzberg, S. L. (2012). Fast gapped-read alignment with Bowtie 2. *Nat. Methods* 9:357–359.

Li, H. (2018). Minimap2: pairwise alignment for nucleotide sequences. *Bioinforma. Oxf. Engl.* 34:3094–3100.

Li, B., and Dewey, C. N. (2011). RSEM: accurate transcript quantification from RNA-Seq data with or without a reference genome. *BMC Bioinformatics* 12:323.

Li, L., Nelson, C. J., Trösch, J., Castleden, I., Huang, S., and Millar, A. H. (2017). Protein degradation rate in *Arabidopsis thaliana* leaf growth and development. *Plant Cell* 29:207–228.

Liu, Y., Schiff, M., Marathe, R., and Dinesh-Kumar, S. P. (2002). Tobacco *Rar1*, *EDS1* and *NPR1/NIM1* like genes are required for *N*-mediated resistance to tobacco mosaic virus. *Plant J.* 30:415–429.

Love, M. I., Soneson, C., and Patro, R. (2018). Swimming downstream: statistical analysis of differential transcript usage following Salmon quantification. *F1000Research* 7:952.

Martínez, F., Sardanyés, J., Elena, S. F., and Daròs, J.-A. (2011). Dynamics of a plant RNA virus intracellular accumulation: stamping machine vs. geometric replication. *Genetics* 188:637–646.

Mergner, J., Frejno, M., List, M., Papacek, M., Chen, X., Chaudhary, A., Samaras, P., Richter, S., Shikata, H., Messerer, M., et al. (2020). Mass-spectrometry-based draft of the *Arabidopsis* proteome. *Nature* 579:409–414.

Metsalu, T., and Vilo, J. (2015). ClustVis: a web tool for visualizing clustering of multivariate data using Principal Component Analysis and heatmap. *Nucleic Acids Res.* 43:W566-570.

Micallef, L., and Rodgers, P. (2014). eulerAPE: drawing area-proportional 3-Venn diagrams using ellipses. *PloS One* 9:e101717.

Nakasugi, K., Crowhurst, R., Bally, J., and Waterhouse, P. (2014). Combining transcriptome assemblies from multiple *de novo* assemblers in the allo-tetraploid plant *Nicotiana benthamiana*. *PloS One* 9:e91776.

Nemhauser, J. L., Hong, F., and Chory, J. (2006). Different plant hormones regulate similar processes through largely nonoverlapping transcriptional responses. *Cell* 126:467–475.

Papp, I., Mur, L. A., Dalmadi, A., Dulai, S., and Koncz, C. (2004). A mutation in the *Cap Binding Protein 20* gene confers drought tolerance to *Arabidopsis*. *Plant Mol. Biol.* 55:679–686.

Pasin, F., Simón-Mateo, C., and García, J. A. (2014). The hypervariable amino-terminus of P1 protease modulates potyviral replication and host defense responses. *PLOS Pathog.* 10:e1003985.

Patro, R., Duggal, G., Love, M. I., Irizarry, R. A., and Kingsford, C. (2017). Salmon provides fast and bias-aware quantification of transcript expression. *Nat. Methods* 14:417–419.

Peart, J. R., Cook, G., Feys, B. J., Parker, J. E., and Baulcombe, D. C. (2002). An *EDS1* orthologue is required for *N*-mediated resistance against tobacco mosaic virus. *Plant J.* 29:569–579.

Pertea, G., and Pertea, M. (2020). GFF utilities: GffRead and GffCompare. *F1000Research* 9:304.

Pertea, M., Pertea, G. M., Antonescu, C. M., Chang, T.-C., Mendell, J. T., and Salzberg, S. L. (2015). StringTie enables improved reconstruction of a transcriptome from RNA-seq reads. *Nat. Biotechnol.* 33:290–295.

Pertea, M., Kim, D., Pertea, G. M., Leek, J. T., and Salzberg, S. L. (2016). Transcript-level expression analysis of RNA-seq experiments with HISAT, StringTie and Ballgown. *Nat. Protoc.* 11:1650–1667.

Robinson, M. D., McCarthy, D. J., and Smyth, G. K. (2010). edgeR: a Bioconductor package for differential expression analysis of digital gene expression data. *Bioinforma. Oxf. Engl.* 26:139–140.

Rodrigo, G., Carrera, J., Jaramillo, A., and Elena, S. F. (2011a). Optimal viral strategies for bypassing RNA silencing. *J. R. Soc. Interface* 8:257–268.

Rodrigo, G., Jaramillo, A., and Blázquez, M. A. (2011b). Integral control of plant gravitropism through the interplay of hormone signaling and gene regulation. *Biophys. J.* 101:757–763.

Rubio, S., Rodrigues, A., Saez, A., Dizon, M. B., Galle, A., Kim, T.-H., Santiago, J., Flexas, J., Schroeder, J. I., and Rodriguez, P. L. (2009). Triple loss of function of protein phosphatases type 2C leads to partial constitutive response to endogenous abscisic acid. *Plant Physiol.* 150:1345–1355.

Correspondence: fpasin@cnb.csic.es

Soneson, C., Love, M. I., and Robinson, M. D. (2015). Differential analyses for RNA-seq: transcript-level estimates improve gene-level inferences. *F1000Research* 4:1521.

Song, L., Huang, S.-S. C., Wise, A., Castanon, R., Nery, J. R., Chen, H., Watanabe, M., Thomas, J., Bar-Joseph, Z., and Ecker, J. R. (2016). A transcription factor hierarchy defines an environmental stress response network. *Science* 354:aag1550.

Suzuki, R., and Shimodaira, H. (2006). Pvclust: an R package for assessing the uncertainty in hierarchical clustering. *Bioinforma. Oxf. Engl.* 22:1540–1542.

The Gene Ontology Consortium (2017). Expansion of the Gene Ontology knowledgebase and resources. *Nucleic Acids Res.* 45:D331–D338.

Thorvaldsdóttir, H., Robinson, J. T., and Mesirov, J. P. (2013). Integrative Genomics Viewer (IGV): high-performance genomics data visualization and exploration. *Brief. Bioinform.* 14:178–192.

Tian, T., Liu, Y., Yan, H., You, Q., Yi, X., Du, Z., Xu, W., and Su, Z. (2017). agriGO v2.0: a GO analysis toolkit for the agricultural community, 2017 update. *Nucleic Acids Res.* 45:W122–W129.

Trincado, J. L., Entizne, J. C., Hysenaj, G., Singh, B., Skalic, M., Elliott, D. J., and Eyras, E. (2018). SUPPA2: fast, accurate, and uncertainty-aware differential splicing analysis across multiple conditions. *Genome Biol.* 19:40.

Umezawa, T., Sugiyama, N., Takahashi, F., Anderson, J. C., Ishihama, Y., Peck, S. C., and Shinozaki, K. (2013). Genetics and phosphoproteomics reveal a protein phosphorylation network in the abscisic acid signaling pathway in *Arabidopsis thaliana*. *Sci. Signal.* 6:rs8.

Wang, P., Xue, L., Batelli, G., Lee, S., Hou, Y.-J., Van Oosten, M. J., Zhang, H., Tao, W. A., and Zhu, J.-K. (2013). Quantitative phosphoproteomics identifies SnRK2 protein kinase substrates and reveals the effectors of abscisic acid action. *Proc. Natl. Acad. Sci. U. S. A.* 110:11205–11210.

Wang, P., Hsu, C.-C., Du, Y., Zhu, P., Zhao, C., Fu, X., Zhang, C., Paez, J. S., Macho, A. P., Tao, W. A., et al. (2020). Mapping proteome-wide targets of protein kinases in plant stress responses. *Proc. Natl. Acad. Sci. U. S. A.* 117:3270–3280.

Yoshida, T., Fujita, Y., Sayama, H., Kidokoro, S., Maruyama, K., Mizoi, J., Shinozaki, K., and Yamaguchi-Shinozaki, K. (2010). AREB1, AREB2, and ABF3 are master transcription factors that cooperatively regulate ABRE-dependent ABA signaling involved in drought stress tolerance and require ABA for full activation. *Plant J.* 61:672–685.

Zhang, R., Calixto, C. P. G., Marquez, Y., Venhuizen, P., Tzioutziou, N. A., Guo, W., Spensley, M., Entizne, J. C., Lewandowska, D., Ten Have, S., et al. (2017). A high quality Arabidopsis transcriptome for accurate transcript-level analysis of alternative splicing. *Nucleic Acids Res.* 45:5061–5073.

Correspondence: fpasin@cnb.csic.es